Dalton Transactions

A spectroscopic, structural, and computational study of Ag-oxo interactions in Ag^{+}/UO_2^{2+}complexes

Journal:	*Dalton Transactions*
Manuscript ID	DT-ART-04-2022-001161.R1
Article Type:	Paper
Date Submitted by the Author:	27-May-2022
Complete List of Authors:	Brager, Dominique; The George Washington University, Department of Chemistry Marwitz, Alexander; Georgetown University, Department of Chemistry Cahill, Chris; The George Washington University, Department of Chemistry

A spectroscopic, structural, and computational study of Ag-oxo interactions in Ag^{+}/UO_2^{2+}complexes

Dominique M. Brager,[a] Alexander C. Marwitz,[b] Christopher L. Cahill[a]

[a]*Department of Chemistry, The George Washington University, 800 22nd Street, NW, Washington, DC, 20052, USA.*
[b]*Department of Chemistry, Georgetown University, Washington, DC, 20057, USA.*

Abstract

Twelve novel Ag^{+}/UO_2^{2+} heterometallic complexes have been prepared and characterized *via* structural, spectroscopic, and computational methods to probe the effects of Ag-oxo interactions on bonding and photophysical properties of the uranyl cation. Structural characterization reveals Ag-oxo interaction distances ranging from 2.475(3) Å to 4.287(4) Å. These interactions were probed using luminescence and Raman spectroscopy which displayed little effect on the luminescence intensity and the energy of the Raman active U=O symmetric stretch peak as compared to previously reported Pb-oxo interactions. Computational efforts *via* density functional theory-based natural bond orbital analysis revealed that the highest stabilization energy associated with the Ag-oxo interaction had a value of only 11.03 kcal/mol and that all other energy values fell at 7.05 kcal/mol or below indicating weaker interactions relative to those previously reported for Pb^{2+}/UO_2^{2+} heterometallic compounds. In contrast, quantum theory of atoms in molecules analysis of bond critical point electron density values indicated *higher* electron density in Ag-oxo interactions as compared to Pb-oxo interactions which suggests more covalent character with the Ag^{+}. Overall, this data indicates that Ag^{+} has a less significant effect on UO_2^{2+} bonding and photophysical properties as compared to other metal cations, likely due to the high polarizability of the cation.

Introduction

The uranyl cation has long been of interest in the actinide community as it is the most environmentally relevant form of uranium due to its high environmental mobility and aqueous solubility.[1,2] More recently there has been an interest in studying heterometallic uranyl complexes to better understand heavy metal effects on the structural assembly, photophysical, and chemical properties of the uranyl cation. Research in this area has shown that secondary metal centers can form interactions with the normally terminal uranyl oxo groups.[1,3–5] The effects of these interactions are of interest as they could be exploited for the purposes of separations and waste stewardship.[6–11]

Arnold et. al. have extensively studied the effects of a wide range of metals including Group 1 and 2 metals, transition metals including Mn^{2+}, Fe^{2+}, Co^{2+}, Pb^{2+}, and Zn^{2+} and some lanthanides on uranyl redox activity using 'pacman' ligand derivatives to engineer close M-oxo interactions.[3,4,12–15] They found that some metal cations are able to weaken and lengthen U=O bonds in the uranyl cation indicated by significant bond asymmetry in the structural information and red-shifting of the Raman active U=O symmetric stretch.[12] In select cases they reported

reduction of U(VI) to U(V) facilitated by metal interaction at the uranyl-oxo.[4,16] A key factor in the magnitude of the effect of the metal cation is the polarizability of the metal where less polarizable (harder) cations had more significant effects on the U=O bond construct.[13]

Previous work done in this group reported on the interactions between the uranyl oxo-group and Pb^{2+} cations.[17] Close Pb-oxo interactions lead to weaker U=O bonds, quenched luminescence, and red-shifting of the U=O symmetric Raman active stretch. Computational analysis determined that the interaction occurred primarily *via* charge transfer between filled Pb *s* and the empty U *5f* and U=O σ^* orbital pairs as well as the filled O sp^x and U=O σ and empty Pb *p* orbital pairs. The transfer of electron density in bonding-relevant orbitals lead to weakening and a loss of covalent character in the U=O bonds interacting with the Pb^{2+} and red-shifting of the U=O symmetric stretch. This charge transfer and disruption of the U=O bond construct likely also lead to changes in the electronic structure of the UO_2^{2+} cation. The change in electronic structure could explain the quenching of the characteristic uranyl luminescence, though the exact mechanism behind the quenching remains unclear. Open-shell transition metals are known to be able to quench uranyl emission through d→d transitions,[18–22] but as this mechanism cannot explain the quenching observed in the Pb^{2+}/UO_2^{2+} complexes.

Our continued efforts explore Ag^+/UO_2^{2+} complexes as Ag^+ also has a closed-shell electron configuration and preparation of bimetallic compounds with the aid of halo-benzoic acid ligands and N-bound capping compounds is straight-forward. The differences between Pb^{2+} and Ag^+ provide an opportunity to further probe how a size, electron configuration, and polarizability might alter the way a metal interacts with the uranyl-oxo and impacts luminescence. Whereas the research by Arnold et. al. suggests that more polarizable metals, like silver, are not as likely to have a significant effect on the uranyl cation, luminescence quenching has been reported for some silver-containing compounds.[23–26] Carter et. al. also reported red-shifting in the Raman active U=O symmetric stretch in compounds with close Ag-oxo contacts, indicating U=O bond weakening.[6]

Herein, we aim to expand on our understanding of how metal cations are able to influence the bonding and spectroscopy of the uranyl cation by studying interactions between Ag^+ cations and the uranyl-oxo group in the solid state. We have synthesized a family of 12 novel Ag^+/UO_2^{2+} containing compounds, adding to the 38 Ag^+/UO_2^{2+} reported in the Cambridge Structural Database (CSD).[27] Our 12 new compounds were characterized structurally, spectroscopically, and computationally to probe the effects of these interactions on bonding and spectroscopy. Through these efforts we demonstrate that the Ag^+ cation has only a very weak effect on uranyl bonding and photophysical properties with only the closest interaction with the Ag^+ cation having a significant effect, likely owing to the lower charge density and higher polarizability of the metal.

Experimental Section

General. *Caution*: Whereas the uranyl nitrate hexahydrate $[UO_2(NO_3)_2]\cdot 6H_2O$ used in this study consists of depleted U, standard precautions for handling radioactive and toxic substances should be followed.

All organic materials, 2,5-dibromobenzoic acid (2,5-diBrBA) (Sigma Aldrich, 96%), 2,5-dichlorobenzoic acid (2,5-diClBA) (Sigma Aldrich, 97%), 4-fluorobenzoic acid (4-FBA) (Acros Organics, 99%), 3-fluorobenzoic acid (3-FBA) (Alfa Aesar, 98%), 3-bromobenzoic acid (3-BrBA) (TCI, 98%), 3-chlorobenzoic acid (3-ClBA) (Sigma Aldrich, 97%), 3,5-dichlorobenzoic acid (3,5-diClBA) (Alfa Aesar, 99%), 2,2';6',2"-terpyridine (terpy) (BeanTown Chemical, 97%), and 2,2'-bipyrimidine (bypm) (Alfa Aesar, 96%), were purchased and used as received. $AgNO_3$ (Alfa Aesar, 99.9+%) is also commercially available and was used without further modification.

Synthesis

All complexes herein were synthesized *via* hydrothermal methods. The halobenzoic acid ligand, N-donor capping ligand (where present), uranyl nitrate, and silver nitrate were used in a 1:1:1:1 ratio and dissolved in 3mL of water. Samples were heated in a 23 mL Teflon-lined Parr autoclave over the course of 3 days and then allowed to cool to room temperature for a few hours before being opened. All samples were rinsed with ethanol and water. Degradation of the 2,2'-bipyrimidine ligand presumably by the mechanism described by Knope et al. resulted in *in-situ* oxalate formation in compounds **4**, **6**, **7**, and **11** leading to multiple phases in some syntheses with one phase integrating the oxalate ligand and another phase without.[28] The organic linkers used in each synthesis and heating temperatures are summarized in Table 1.

Table 1. Summary of synthesis conditions of complexes 1-12.

Compound(s)	Temperature (°C)	Halobenzoic acid	N-Donor Cap
1	110	2,5-dibromobenzoic acid	None
2	110	2,5-dichlorobenzoic acid	2,2'-bipyrimidine
3	110	2,5-dibromobenzoic acid	2,2'-bipyrimidine
4 and 10	110	4-fluorobenzoic acid	2,2'-bipyrimidine
5	110	3-fluorobenzoic acid	2,2';6',2"-terpyridine
6	150	2,5-dichlorobenacoic acid	2,2'-bipyrimidine
7 and 8	110	3-bromobenzoic acid	2,2'-bipyrimidine
9	110	3-chlorobenzoic acid	2,2'-bipyrimidine
11	110	3-fluorobenzoic acid	2,2'-bipyrimidine
12	110	3,5-dichlorobenzoic acid	2,2'-bipyrimidine

X-ray Crystallography. Single crystals from each bulk sample were isolated and mounted on MiTeGen micromounts. Data were collected on a Bruker D8 Quest equipped with a Photon II detector, using a Mo Kα source. Reflection data were collected using 0.5°ω and φ scans at 100(2) K. The APEX III software suite[29,30] was used for integrating reflection data and performing absorption corrections, which incorporates both SAINT[31] and SADABS.[32] Structure solutions (obtained using intrinsic phasing) and refinement were performed using the ShelXT package[33] and ShelXL[34] in APEX III.[31] For compound **6**, a differential absorption correction method was applied as multi-scan alone is not suitable for highly absorbing non-isotropic crystals.[35]All non-hydrogen atoms were located using Fourier difference maps and refined anisotropically. Hydrogen atoms

were placed in ideal locations using HFIX33 for methyl groups, and HFIX43 for aromatic hydrogen atoms, allowing hydrogen atoms to ride on their parent atoms. All figures were prepared with Crystal Maker 8.2.2.[36] Data collection and refinement details for **1–12** are included in Table 2 and thermal ellipsoid plots for each structure are included in the SI (Figure S1-S12).

In compound **5** a DAMP command was issued due to a highly disordered and partially occupied solvent water molecule.

Table 2. Crystallographic Refinement Details for Compounds 1−12.[a]

	1	**2**	**3**
CCDC no.	2160088	2160089	2160090
Formula	$[UO_2Ag(C_7H_3Br_2O_2)_3]$	$[(UO_2)_{1.5}Ag_2(C_8H_3N_2)_2(C_7H_3Cl_2O_2)NO_3][UO_2(C_7H_3Cl_2O_2)_3]$	$[(UO_2)_{1.5}Ag_2(C_8H_3N_2)_2(C_7H_3Br_2O_2)NO_3][UO_2(C_7H_3Br_2O_2)_3]$
Formula weight	1214.58	3518.22	4229.42
Crystal System	Monoclinic	Triclinic	Triclinic
Space Group	$P2_1/n$	P-1	P-1
a, Å	12.9345(5)	11.3416(11)	11.4685(6)
b, Å	11.7271(5)	11.9769(11)	12.0683(6)
c, Å	17.4596(8)	20.173(2)	20.6348(10)
α, °	90	90.192(4)	91.656(2)
β, °	95.082(2)	104.416(3)	104.090(2)
γ, °	90	100.396(3)	101.520(2)
Volume, Å^3	3637.93(19)	2607.0(4)	2705.2(2)
Z	4	1	1
ρ_{calc}, g cm^{-3}	3.058	2.241	2.596
μ, mm^{-1}	16.008	5.872	11.173
Radiation	0.71073	0.71073	0.71073
Temp., K	100	100	100
residuals:[a] R; R_w	0.0276, 0.0703	0.0301, 0.0547	0.0266, 0.0590
Goodness of fit	1.074	1.022	1.015
	4	**5**	**6**
CCDC no.	2160091	2160092	2160093
Formula	$[Ag(C_8H_3N_2)H_2O][UO_2(C_7H_5FO_2)(C_2O_4)]$	$[UO_2Ag_2(C_{15}H_{11}N_3)_2(C_7H_5FO_2)_3][UO_2(C_7H_5FO_2)_3] \cdot H_2O$	$[Ag(C_8H_3N_2)][UO_2(C_7H_3Cl_2O_2)(C_2O_4)]$
Formula weight	781.21	4131.81	814.08
Crystal System	Monoclinic	Triclinic	Triclinic
Space Group	C2/c	P-1	P-1
a, Å	16.8738(6)	10.3400(6)	9.0510(13)
b, Å	11.6376(4)	19.0906(11)	10.4720(14)
c, Å	20.8532(9)	20.2806(12)	12.0195(16)
α, °	90	64.177(2)	99.151(5)
β, °	91.685(1)	75.436(2)	98.695(5)
γ, °	90	79.015(2)	107.432(5)
Volume, Å^3	4093.2(3)	3472.7(4)	1048.9(3)
Z	8	1	2
ρ_{calc}, g cm^{-3}	2.535	1.976	2.578
μ, mm^{-1}	8.929	5.295	8.953
Radiation	0.71073	0.71073	0.71073
Temp., K	100	100	100
residuals:[a] R; R_w	0.0149, 0.0344	0.0259, 0.0564	0.0423, 0.1010
Goodness of fit	1.095	1.031	1.031
	7	**8**	**9**
CCDC no.	2160094	2160095	2160096
Formula	$[Ag(C_8H_3N_2)][UO_2(C_7H_5BrO_2)(C_2O_4)]$	$[Ag(C_8H_3N_2)][UO_2(C_7H_5BrO_2)_3]$	$[Ag(C_8H_3N_2)][UO_2(C_7H_5ClO_2)_3]$

Formula weight	824.09	2272.15	1002.72
Crystal System	Triclinic	Monoclinic	Monoclinic
Space Group	P-1	$P2_1/c$	$P2_1/c$
a, Å	8.9506(3)	14.384(3)	14.2027(4)
b, Å	10.6865(4)	17.836(4)	17.9512(5)
c, Å	12.1235(5)	12.181(2)	12.1626(4)
α, °	102.007(1)	90	90
β, °	103.825(1)	98.66(3)	97.402(1)
γ, °	108.310(1)	90	90
Volume, Å^3	1017.36(7)	3089.5(11)	3075.08(16)
Z	2	2	4
ρ_{calc}, g cm^{-3}	2.690	2.443	2.166
μ, mm^{-1}	10.930	9.807	6.215
Radiation	0.71073	0.71073	0.71073
Temp., K	100	100	100
residuals:[a] R; R_w	0.0234, 0.0438	0.0452, 0.1049	0.0252, 0.0566
Goodness of fit	1.052	1.071	1.107
	10	**11**	**12**
CCDC no.	2160097	2160098	2160099
Formula	$[Ag_2(C_8H_3N_2)]_2[UO_2(C_7H_5FO_2)_2NO_3]$	$[Ag(C_8H_3N_2)][UO_2(C_7H_5FO_2)(C_2O_4)]$	$[UO_2Ag(C_8H_3N_2)_{0.5}(C_7H_3Cl_2O_2)_3]$
Formula weight	1222.35	984.48	1026.97
Crystal System	Orthorhobmic	Triclinic	Triclinic
Space Group	Pccn	P-1	P-1
a, Å	17.6419(10)	9.7834(3)	10.0976(6)
b, Å	33.4658(19)	9.9477(3)	10.5315(6)
c, Å	12.2346(7)	11.9626(3)	15.7506(9)
α, °	90	100.009(1)	98.640(2)
β, °	90	111.546(1)	90.851(2)
γ, °	90	106.752(1)	118.043(2)
Volume, Å^3	7223.3(7)	984.48(5)	1454.51(15)
Z	8	2	2
ρ_{calc}, g cm^{-3}	2.248	2.575	2.345
μ, mm^{-1}	5.637	9.274	6.837
Radiation	0.71073	0.71073	0.71073
Temp., K	100	100	100
residuals:[a] R; R_w	0.0192, 0.0435	0.0226, 0.0434	0.0221, 0.0443
Goodness of fit	1.111	1.033	1.037

Powder X-Ray Diffraction. Powder X-Ray Diffraction (PXRD) data on the bulk reaction products of compounds **1-9** and **12** (Figure S14-S22) were used to assess the purity of the preparations. All data were collected on a Rigaku Miniflex (Cu Kα, 2θ = 3-60°) and were analyzed using the Match! software program.[37] Compounds **10** and **11** were minor phases and did not appear in high enough yield to perform PXRD analysis. Compounds **2, 3, 6,** and **9** resulted in pure phases. Compounds **7** and **8** were prepared in the same synthesis and both phases were identified in the powder pattern. While compounds **4** and **10** were prepared in the same synthesis, **10** did not have a high enough yield to appear in the powder pattern. This synthesis also resulted in another phase that did correspond to any of the known reactants or impurities. Syntheses of compounds **1** and **5** also resulted in additional phases that did not correspond to any known reactants or impurities and as such we were unable to identify these phases. The synthesis of compound **12** resulted in a biphasic mixture of **12** and an additional Ag^+/bypm phase ($[Ag(C_8H_6N_4)]\ NO_3 \bullet H_2O$) which was identified from the CSD (Refcode: YABDIQ).[38]

Optical Measurements. Steady-state luminescence scans of **3-6, 8-12** were collected at 298 K and 78 K. Spectra were collected with a Fluorolog®-3 photoluminescence spectrophotometer from Horiba using a 450 W xenon arc lamp combined with a double excitation monochromator and double emission monochromator. A photomultiplier tube at 950 V was used as the emission detector. Crystalline samples (purity confirmed by SCXRD) were mounted on a quartz plate using non-emitting high vacuum grease. Raman spectra of single crystals of **1-12** were collected using a HORIBA LabRAM HR Evolution Raman Microscope over the 50–2000 cm−1 range. An excitation line at 405 nm was used for each collection.

Computational details.

Natural Bond Orbitals (NBO) and Quantum Theory of Atoms in Molecules (QTAIM). The uranyl-cation interactions in **1-12** between the UO_2^{2+} and Ag^+ units were investigated and quantified via Density Functional Theory as implemented in Gaussian 16.[39] Single point energy calculations were performed on models of **1-12** constructed directly from unoptimized crystallographic fragments consisting of the closest Ag-oxo interaction and all ligands coordinated to the Ag^+ and UO_2^{2+} using the B3LYP[40,41] functional, which has been shown to reproduce experimental parameters of uranyl complexes with high accuracy.[42,43] The modified scalar-relativistic effective core potential (ECP) basis set DEF2TZVP[44,45] and associated pseudopotential for all non-U atoms was implemented in the software was used throughout. The ECP60MWB and ECP60MWB_SEG valence basis set was used for all U atoms.[46–48] No additional corrections were used for the energy calculations and a tight convergence criterion was used. Natural Localized Molecular Orbitals were obtained from converged wavefunctions. Second order perturbation theory (SOPT) was applied to (i) quantify the magnitude of the interaction (in kcal/mol) between the donor and acceptor and (ii) identify particular natural bonding molecular orbitals involved. Quantum theory of atoms in molecules[48] (QTAIM) analysis of bonding properties at the bond critical points (BCPs) was performed in the AIMA11 software suite[49] using the DFT converged wavefunction. Models generated and used for NBO and AIMA11 calculations can be found in the SI (Figure S13) along with a sample input file (Sample S1).

Results and Discussion

Structural Descriptions.

Compound **1**, $[UO_2Ag(2,5\text{-diBrBA})_3]$, crystallizes in the space group $P2_1/n$ and the asymmetric unit contains a single crystallographically unique UO_2^{2+} cation adopting a pentagonal bipyramidal geometry as well as one crystallographically unique six-coordinate Ag^+ cation (Figure 1). The axial U=O bonds have bond lengths of 1.761(3) Å (O1) and 1.781(3) Å (O2) with a ∠O-U-O of 179.1(1)°. The UO_2^{2+} cation is coordinated in the equatorial plane by one bidentate 2,5-dibromobenzoate ligand (*via* O5, and O6) and by three monodentate 2,5-dibromobenzoate ligand (*via* O7, O8, and O3). The Ag^+ cation forms a bidentate coordination with a 2,5-dibromobenzoate

ligand *via* O4 and Br2. The carboxylate group containing O3 and O4 bridges the Ag^{+} cation to the UO_2^{2+} cation. Additionally, the Ag^{+} cation is coordinated to Br3 on a 2,5-dibromobenzoate ligand which is coordinated to the UO_2^{2+} cation *via* O6 and O5. The Ag^{+} cation also has a close interaction with a crystallographically equivalent Ag^{+} cation at a distance of 3.303(1) Å. The Ag^{+} cation interacts with one of the oxo groups of the UO_2^{2+} cation *via* O2 with a distance of 2.475(3) Å and a ∠U-O-Ag angle of 127.0(2)°. Packing of **1** (Figure 2) features 1-dimensional UO_2^{2+} and Ag^{+} cation chains in the [100] direction which are assembled *via* halogen bonding interactions between Br atoms on adjacent 2,5-dibromobenzoate molecules.

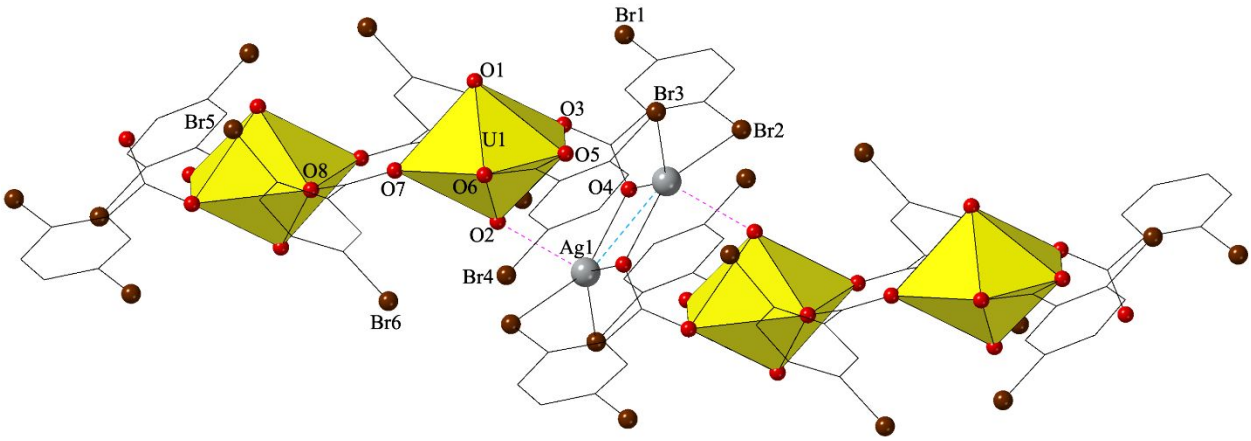

Figure 1. Local representation of compound **1** detailing the metal coordination environments. Uranyl polyhedra are shown in yellow; Ag, Br, and O are grey, brown, and red spheres respectively. Silver-oxo interaction depicted by a dotted pink line and close Ag-Ag distance is depicted by a light blue line. H atoms have been omitted for clarity.

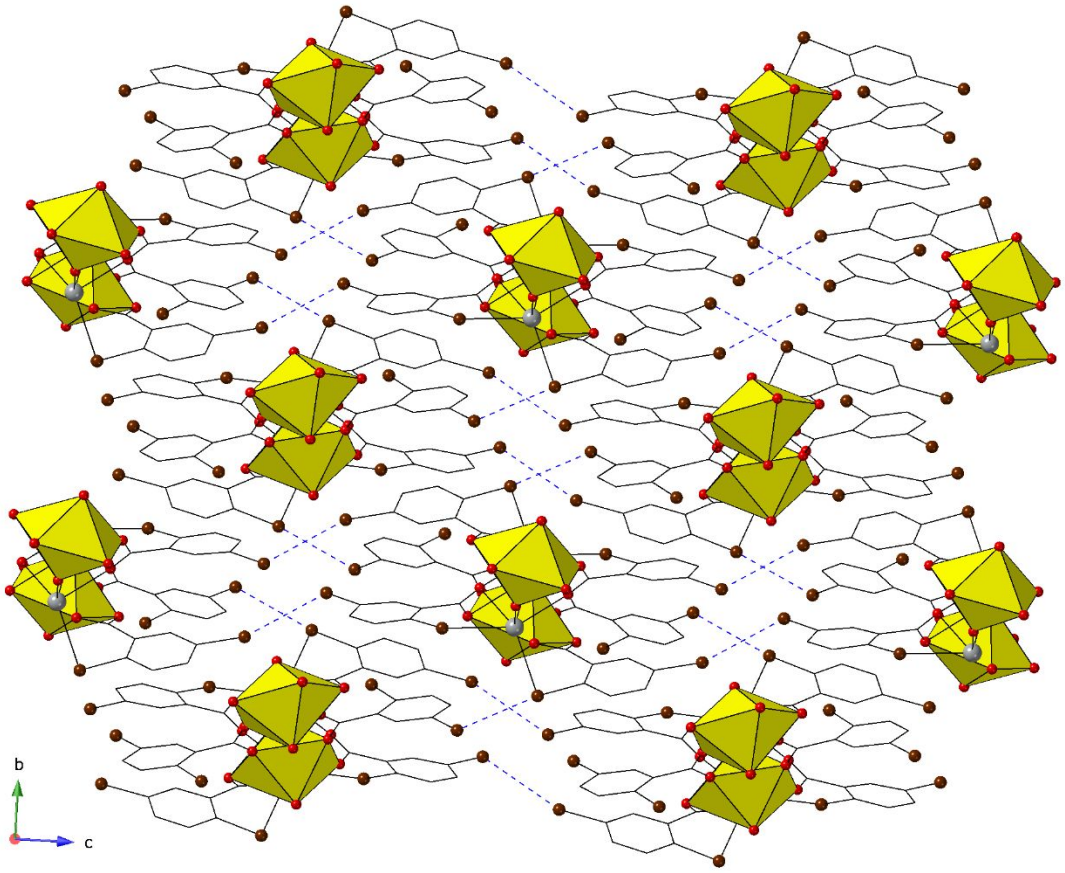

Figure 2. Global structure of **1** shown along the *a*-axis. Halogen bonding between Br atoms on adjacent 2,5-dibromobenzoate ligands is depicted by the dotted blue lines.

Compound **2**, $[(UO_2)_{1.5}Ag_2(bypm)_2(2,5\text{-diClBA})NO_3][UO_2(2,5\text{-diClBA})_3]$, crystallizes in the space group *P-1* and the asymmetric unit features two crystallographically unique UO_2^{2+} cations both adopting a hexagonal bipyramidal geometry (Figure 3). One UO_2^{2+} cation (U2, O2, and O3) displays bidentate coordination to three 2,5-dichlorobenzoate ligands (*via* O9 and O10, O11 and O12, O13 and O14) in the equatorial plane forming a monomeric unit. This unit has U=O bond distances of 1.774(3) Å and 1.760(3) Å with an ∠O-U-O of 179.1(1)°. The second UO_2^{2+} cation also forms a monomeric unit, where U1 lies on an inversion center, with U=O bond lengths of 1.767(2) Å and an ∠O-U-O of 180°. It is coordinated by two crystallographically equivalent monodentate 2,5-dicholorobenzoate ligands *via* O4. Additionally, it is coordinated by two crystallographically equivalent monodentate nitrate groups *via* O6 and O7. The asymmetric unit also contains two Ag^+ cations (Ag1 and Ag2). Ag1 forms a close interaction with the UO_2^{2+} cation containing U1 at a distance of 2.645(3) Å and a ∠U-O-Ag of 137.1(2)°. Both Ag^+ cations are coordinated by two bipyrimidine ligands forming 1-dimensional chains along the [010] direction. The UO_2^{2+} monomers containing U2 interact with each other *via* π-π interactions between 2,5-dicholorobenzoate ligand rings on adjacent units (Figure 4). The UO_2^{2+} monomers containing U1 interact *via* halogen bonding between Cl atoms on adjacent units.

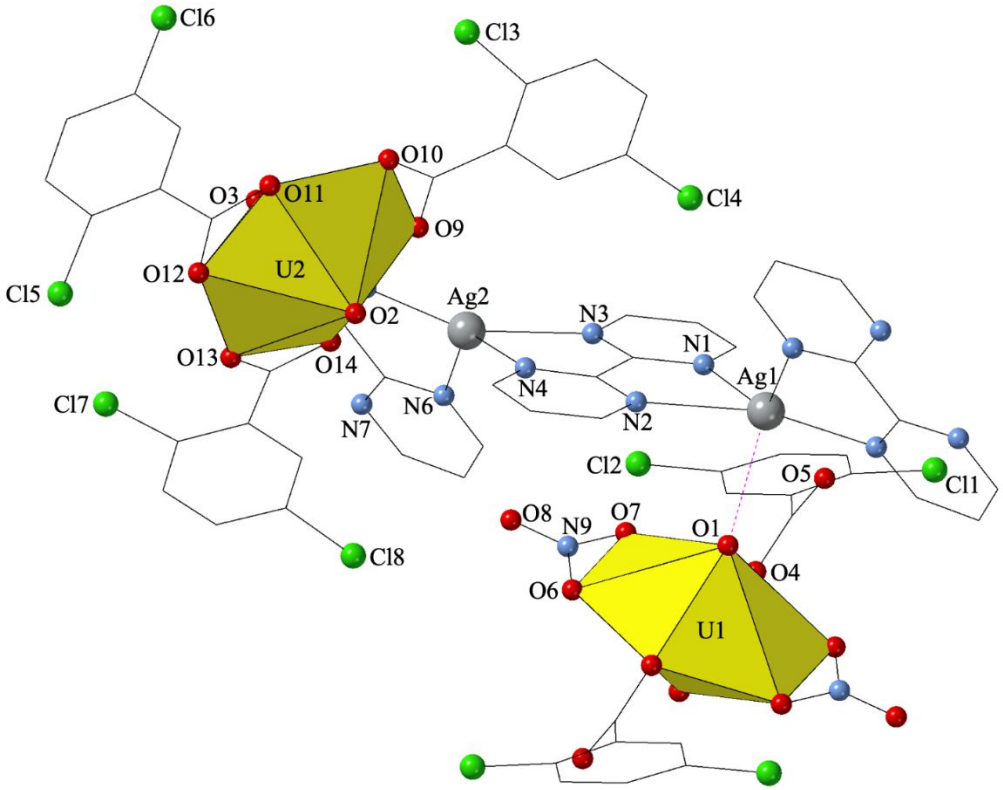

Figure 3. Local representation of compound **2** detailing the metal coordination environments. Cl and N are green and blue spheres respectively.

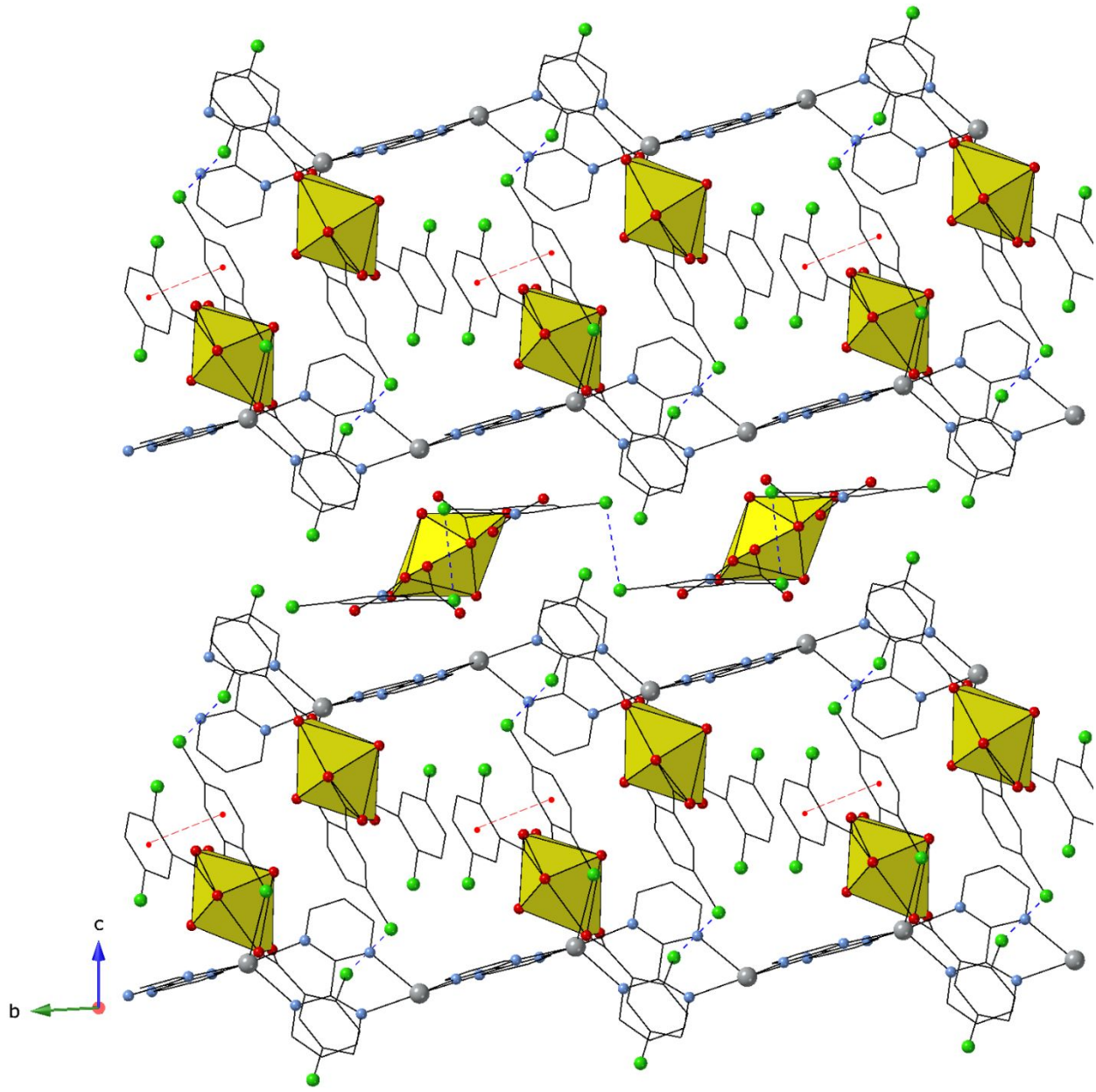

Figure 4. Global structure of compound **2** shown along the *a*-axis. Halogen bonding between Cl atoms on adjacent 2,5-dichlorobenzoate ligands is depicted by the dotted blue lines. π-π interactions between 2,5-dicholorobenzoate centroids is depicted by red dotted lines.

Compound **3**, $[(UO_2)_{1.5}Ag_2(bypm)_2(2,5\text{-diBrBA})NO_3][UO_2(2,5\text{-diBrBA})_3]$, is isostructural to compound **2**. The UO_2^{2+} cation containing U2 has U=O bond lengths of 1.774(3) and 1.763(3), and an ∠O-U-O of 179.1(1)° (Figure 5). The UO_2^{2+} cation containing U1 has U=O bond lengths of 1.773(1) Å and an ∠O-U-O of 180°. The Ag-O distance with the UO_2^{2+} containing U1 is 2.647(3) Å and has a ∠U-O-Ag of 135.9(2)°. (Global structure can be seen in Figure 6)

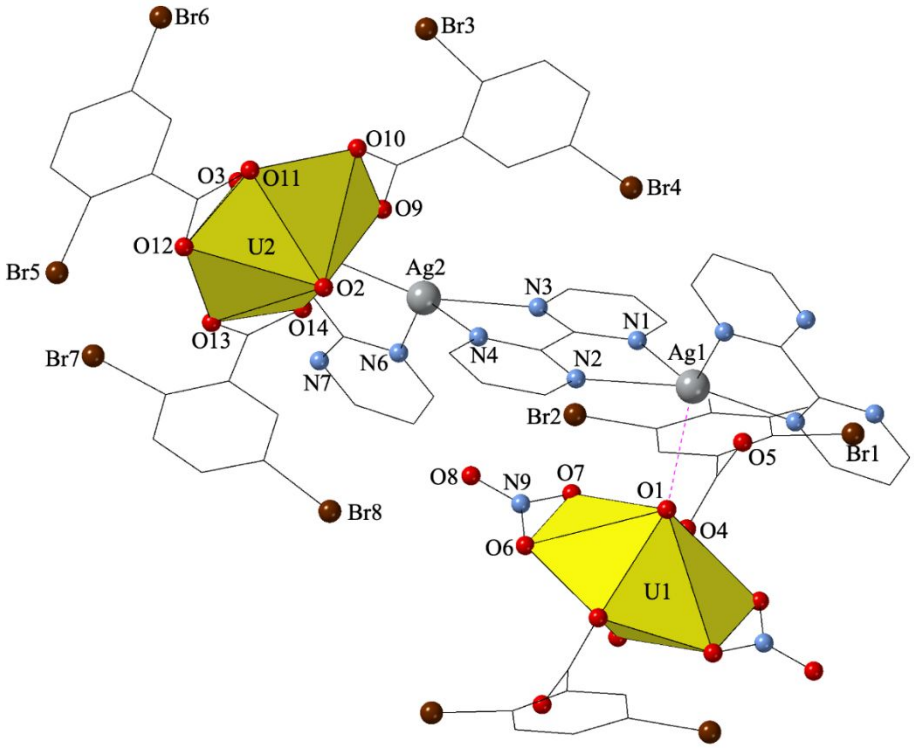

Figure 3. Local representation of compound **3** detailing the metal coordination environments.

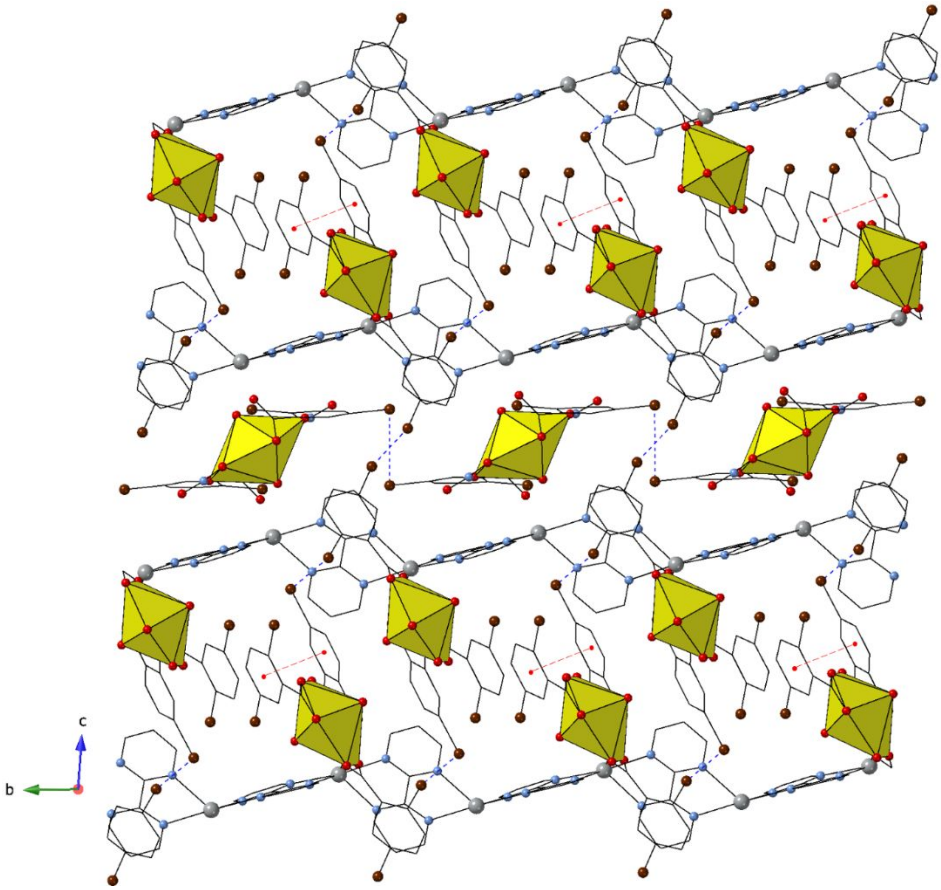

Figure 6. Global structure of compound **2** shown along the *a*-axis. Halogen bonding between Br atoms on adjacent 2,5-dibromobenzoate ligands is depicted by the dotted blue lines. π-π interactions between 2,5-dibromobenzoate centroids is depicted by red dotted lines.

Compound **4**, $[Ag(bypm)H_2O][UO_2(4\text{-}FBA)(Ox)]$, crystallizes in the space group *C2/c* and the asymmetric unit contains a single crystallographically unique UO_2^{2+} cation adopting a pentagonal bipyramidal geometry as well as one crystallographically unique five-coordinate Ag^+ cation (Figure 7). The axial U=O bonds have bond lengths of 1.772(3) Å (O1) and 1.778(2) Å (O2) with a ∠O-U-O of 177.9(1)°. The UO_2^{2+} cation is coordinated in the equatorial plane by two crystallographically equivalent bidentate oxalate ligands (*via* O1 and O2) and by one monodentate 4-fluorobenzoate ligand. The oxalate ligands bridge UO_2^{2+} cations to form 1-dimensional chains along the [010] direction. The Ag^+ cation is coordinated by one water molecule (O9) and forms a bidentate coordination with two 2,2'-bipyrimidine ligands *via* N1, N2, N3 and N4. The 2,2'-bipyrimidine ligands each coordinate to other Ag^+ cations, forming 1-dimensional chains in the [001] direction. Adjacent UO_2^{2+} chains pack *via* halogen bonding between fluorine atoms on adjacent 4-fluorobenzoate ligands. The water coordinated to the Ag^+ cation (O9) forms a hydrogen bond with O4 on a 4-fluorobenzoate ligand carboxylate group (Figure 8). The UO_2^{2+} and Ag^+ chains are held together by close interactions between the Ag^+ cations and the uranyl oxo groups (O1). These interactions have a distance of 2.742(2) Å and a ∠U-O-Ag angle of 140.71(9)°.

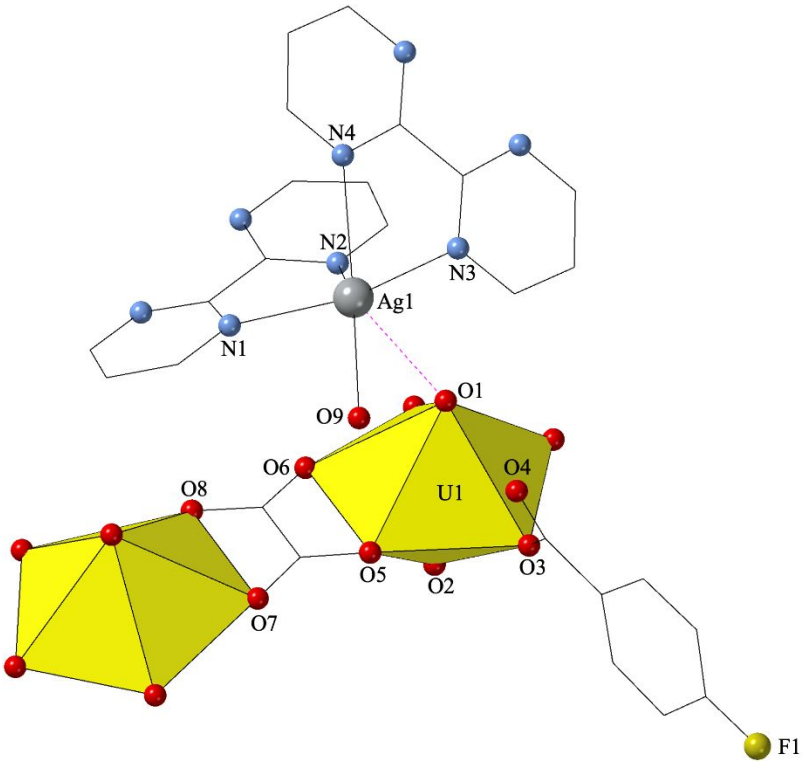

Figure 7. Local representation of compound **4** detailing the metal coordination environments. F atoms are represented by yellow spheres.

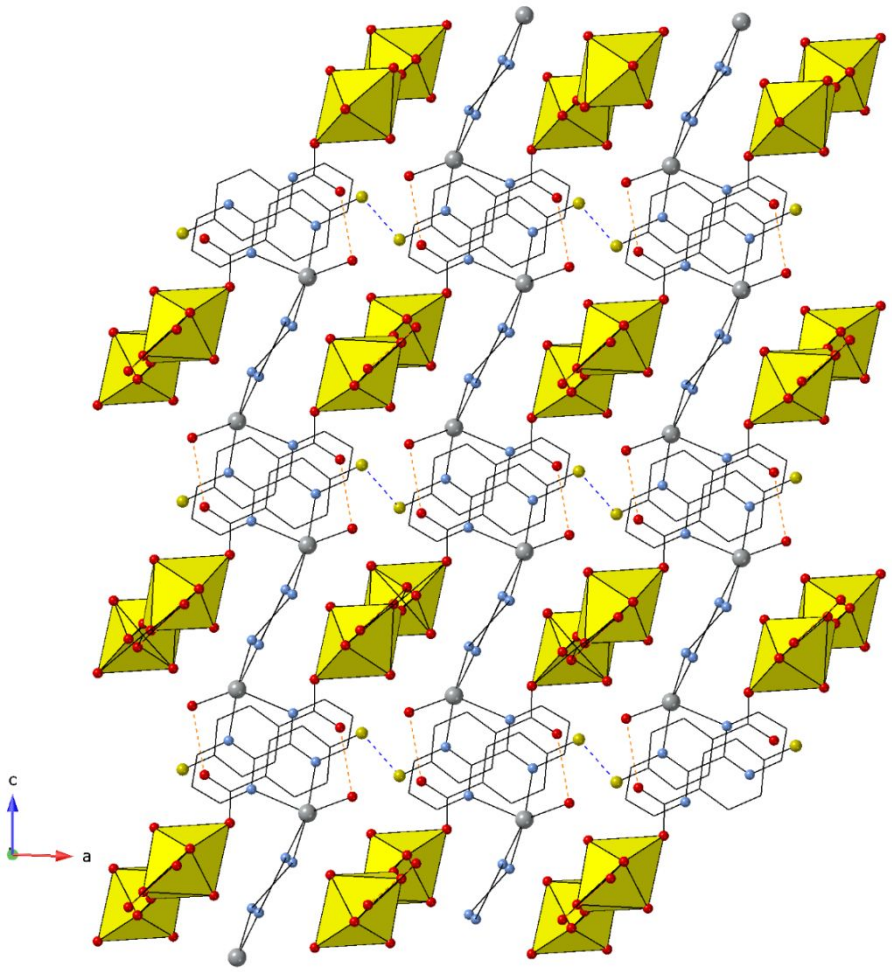

Figure 8. Global structure of compound **4** shown along the *b*-axis. Halogen bonding between F atoms on adjacent 4-fluorobenzoate ligands is depicted by the dotted blue lines. Hydrogen bonds are depicted by orange dotted lines.

Compound **5**, $[UO_2Ag_2(terpy)_2(3\text{-}FBA)_3][UO_2(3\text{-}FBA)_3] \bullet H_2O$, crystallizes in the space group *P-1* and the asymmetric unit contains two crystallographically unique UO_2^{2+} cations, an Ag^+ cation, and a lattice water molecule (Figure 9). The UO_2^{2+} cation containing U2 adopts a hexagonal bipyramidal geometry with U=O bond lengths of 1.776(3) Å and 1.772(3) Å with a ∠O-U-O of 178.9(1)°. It is coordinated in the equatorial plane by three bidentate 3-fluorobenzoate ligands (*via* O11 and O12, O13 and O14, O15 and O16). The other UO_2^{2+} cation (containing U1) adopts a pentagonal bipyramidal geometry where axial U=O bonds have bond lengths of 1.776(3) Å (O1) and 1.773(3) Å (O2) with a ∠O-U-O of 179.4(1)°. U1 is coordinated in the equatorial plane by one bidentate and three monodentate 3-fluorobenzate ligands. One of the 3-fluorobenzoate ligands (containing O9) coordinates to another UO_2^{2+} cation *via* O10 to form a dimeric unit. The Ag^+ cation

is coordinated two tridentate 2,2';6',2"-terpyridine ligands (*via* N1, N2, and N3, and N4, N5, and N6) and is also bridged to the UO_2^{2+} cation containing U1 *via* a 3-fluorobenzoate ligand (O8) (Figure 10). The Ag^+ cation additionally displays a close interaction with the oxo group of the UO_2^{2+} cation containing U1 at a distance of 2.875(2) Å and a ∠U-O-Ag angle of 115.1(1)°.

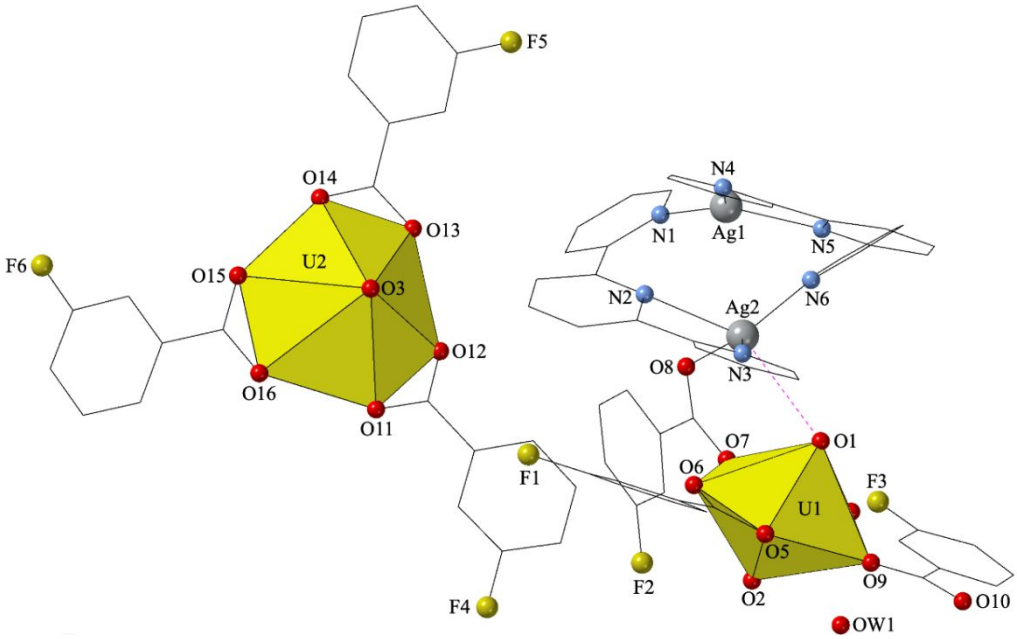

Figure 9. Local representation of compound **5** detailing the metal coordination environments.

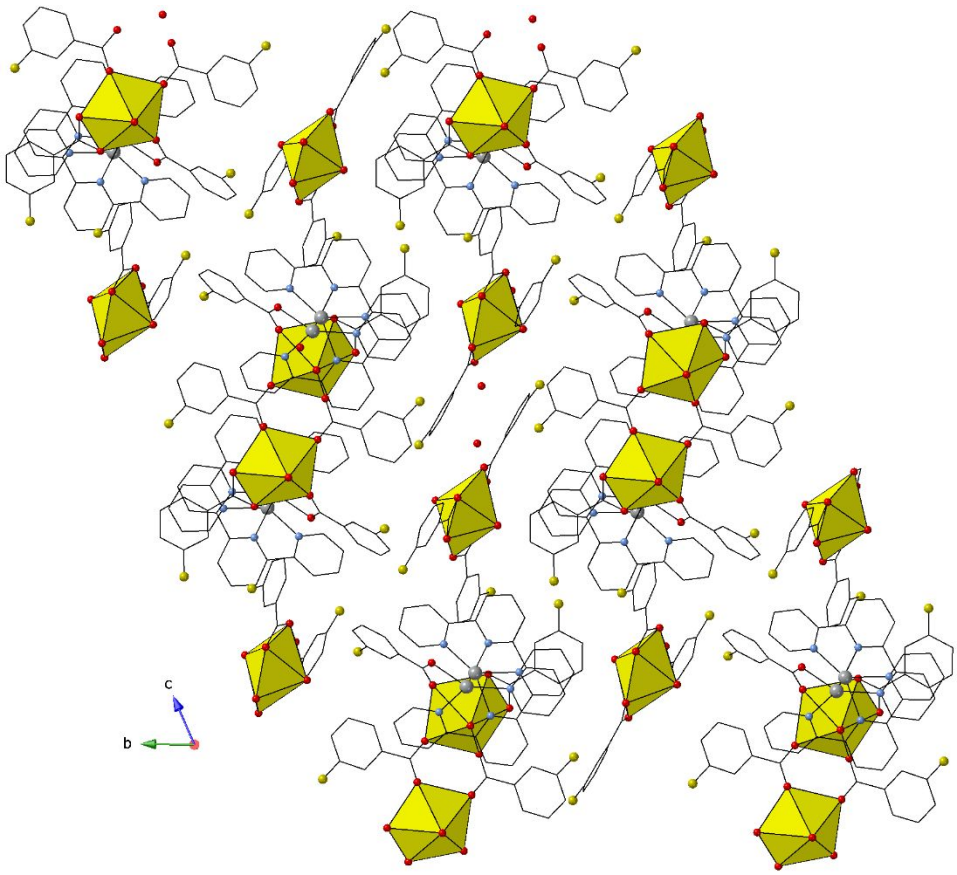

Figure 10. Global structure of compound **5** shown along the *a*-axis.

Compound **6**, [Ag(bypm)][UO_2(2,5-diClBA)(Ox)], crystallizes in the space group *P-1* and the asymmetric unit contains a single crystallographically unique UO_2^{2+} cation adopting a pentagonal bipyramidal geometry as well as one crystallographically unique four-coordinate Ag^+ cation (Figure 11). The UO_2^{2+} cation is coordinated in the equatorial plane by two crystallographically equivalent bidentate oxalate ligands (*via* O1 and O2) and by one monodentate 2,5-dichlorobenzoate ligand. The oxalate ligands bridge UO_2^{2+} cations to form 1-dimensional chains along the [010] direction. The axial U=O bonds have bond lengths of 1.769(6) Å (O2) and 1.773(5) Å (O1) with a ∠O-U-O of 178.7(2)°. The Ag^+ cation forms a bidentate coordination with two 2,2'-bipyrimidine ligands *via* N1, N2, N3 and N4. The 2,2'-bipyrimidine ligands each coordinate to other Ag^+ cations, forming 1-dimensional chains in the [001] direction (Figure 12). The UO_2^{2+} and Ag^+ chains are held together by close interactions between the Ag^+ cations and the uranyl oxo groups (O2). These interactions have a distance of 2.932(7) Å and a ∠U-O-Ag angle of 141.7(3)°.

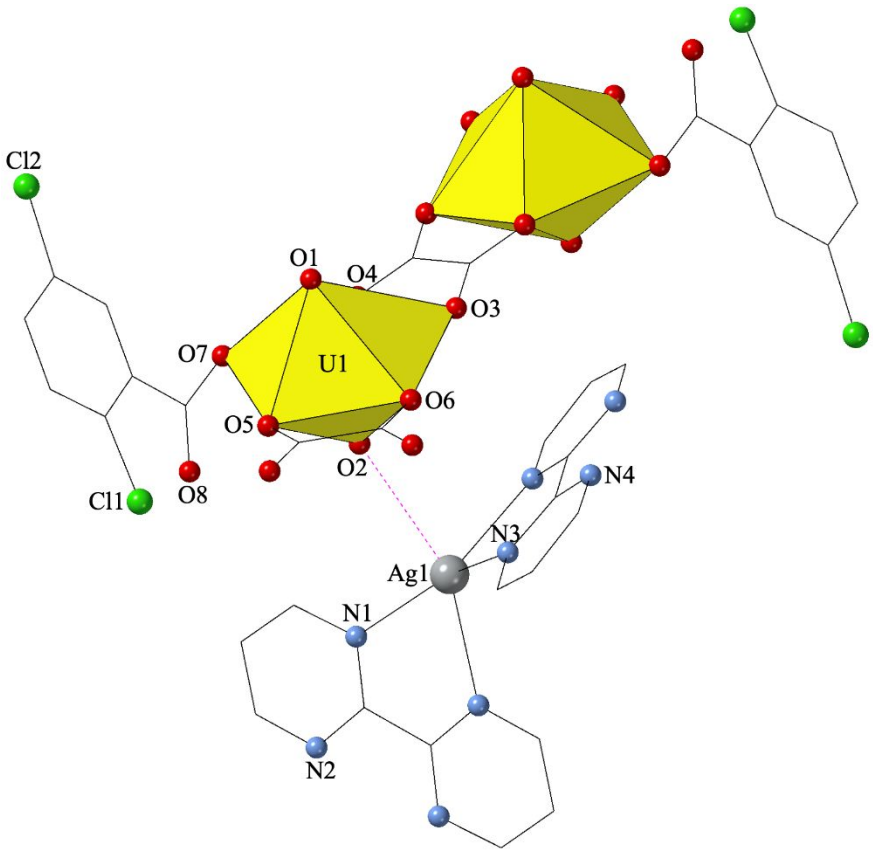

Figure 11. Local representation of compound **6** detailing the metal coordination environments.

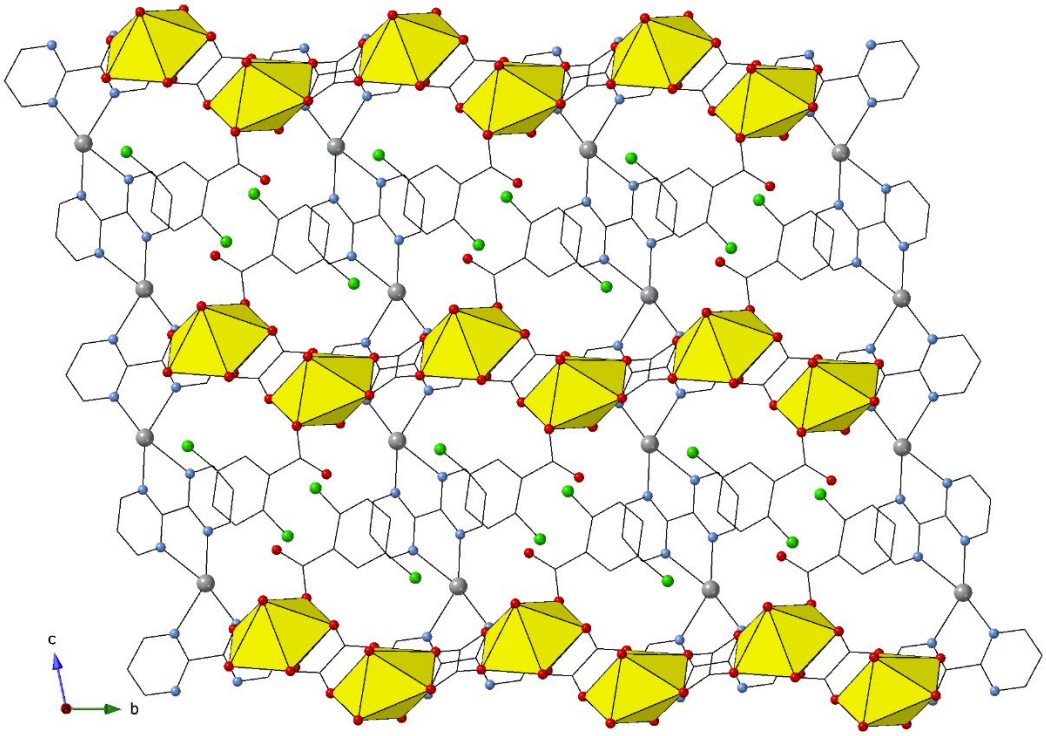

Figure 12. Global structure of compound **6**.

Compound **7**, [Ag(bypm)][UO_2(3-BrBA)(Ox)], is isomorphous to compound **6** with differences in the number and positioning of halogens; compound **6** has two chlorine atoms in the 2 and 5 positions, and **7** has one bromine atom at the 1 position. Despite the differences in the halogens, the two compounds experience similar packing. The UO_2^{2+} cation has U=O bond lengths of 1.769(6) Å (O2) and 1.771(4) Å (O1) and an ∠O-U-O of 178.6(2)° (Figure 13). The Ag-O distance is 3.093(4) Å and has a ∠U-O-Ag of 143.0(2)°. (Global structure can be seen in Figure 14).

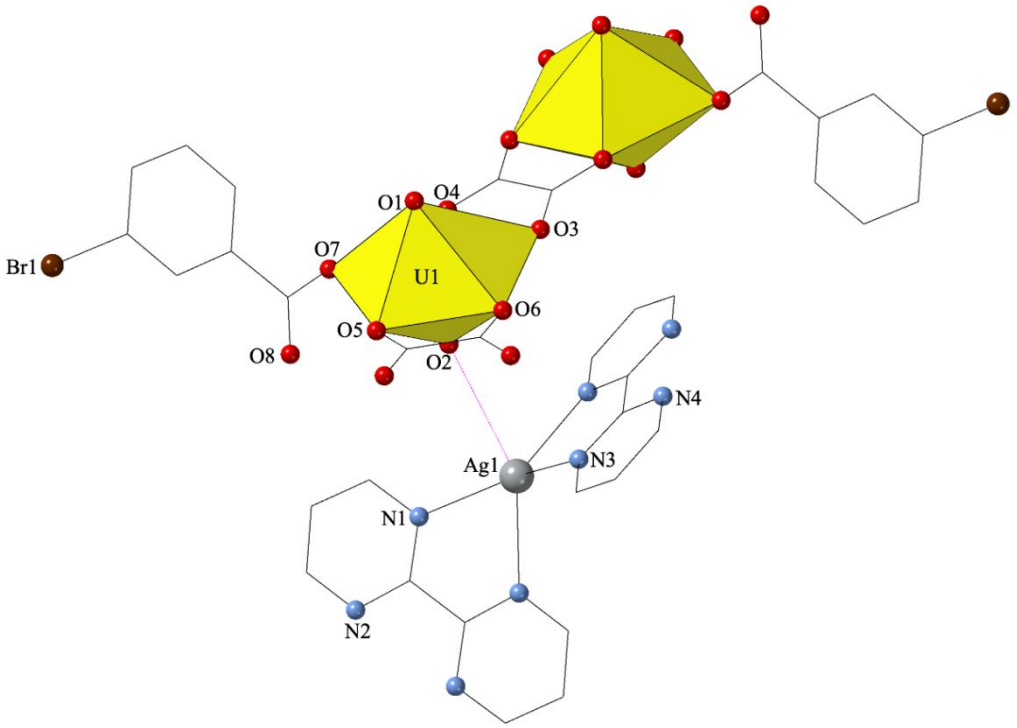

Figure 13. Local representation of compound **7** detailing the metal coordination environments.

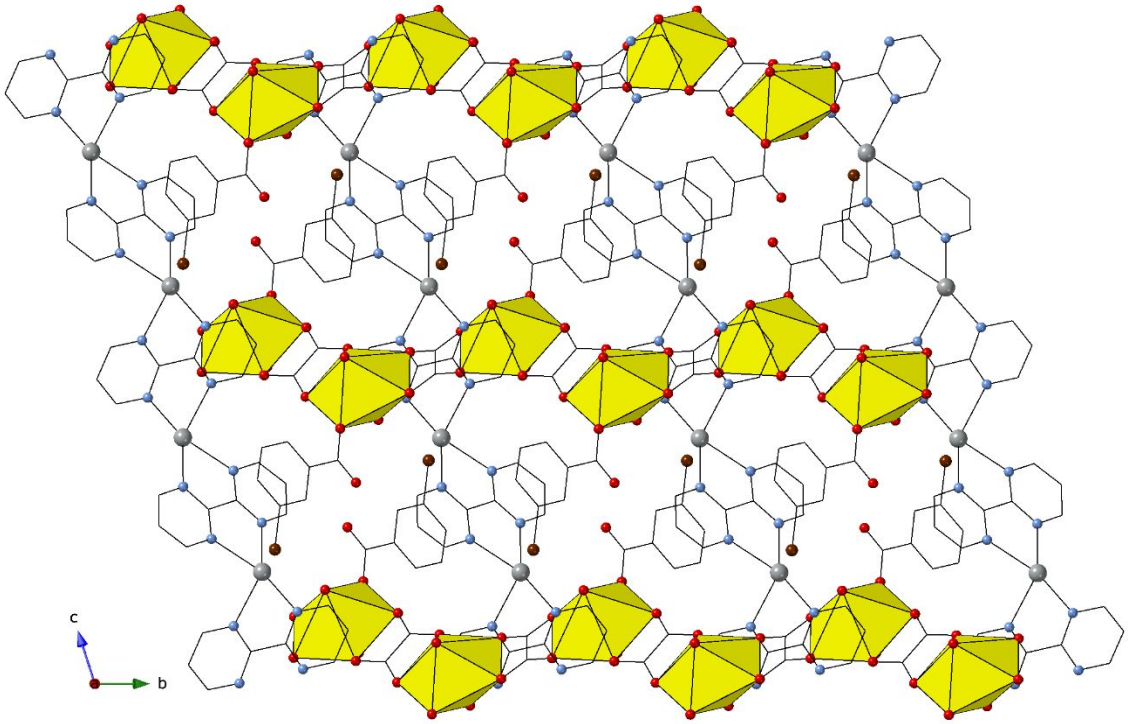

Figure 14. Global structure of compound **7**.

Compound **8**, [Ag(bypm)][UO_2(3-BrBA)$_3$], crystallizes in the space group *P2$_1$/c* and the asymmetric unit contains a single crystallographically unique UO_2^{2+} cation adopting a hexagonal bipyramidal geometry as well as one crystallographically unique four-coordinate Ag^+ cation (Figure 15). The UO_2^{2+} cation is coordinated in the equatorial plane by three bidentate 3-bromobenzoate ligands forming a monomeric unit. The axial U=O bonds have bond lengths of 1.766(5) Å (O1) and 1.752(5) Å (O2) with a ∠O-U-O of 179.1(3)°. The Ag^+ cation displays bidentate coordination with two 2,2'-bipyrimidine ligands *via* N1, N2, N3 and N4. The 2,2'-bipyrimidine ligands each coordinate to other Ag^+ cations, forming 1-dimensional chains in the [001] direction (Figure 16). Additionally, the uranyl monomers are assembled *via* halogen bonding interactions between bromine atoms on adjacent 3-bromobenzoate ligands. The Ag-O distance is 3.314(6) Å and the ∠U-O-Ag is 171.8(3)°.

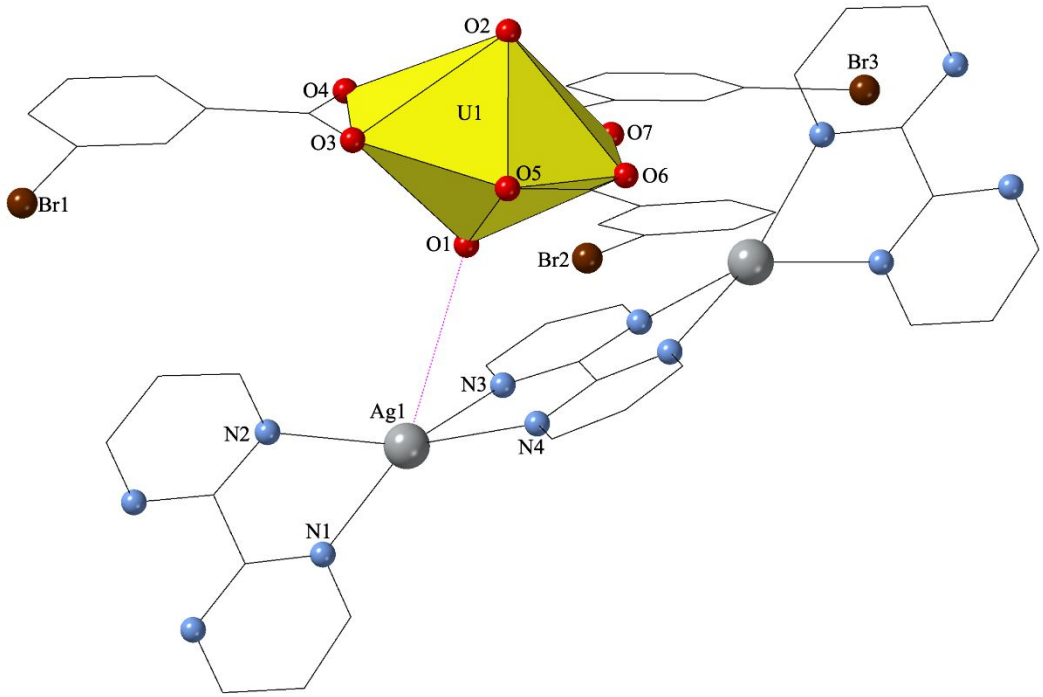

Figure 15. Local representation of compound **8** detailing the metal coordination environments.

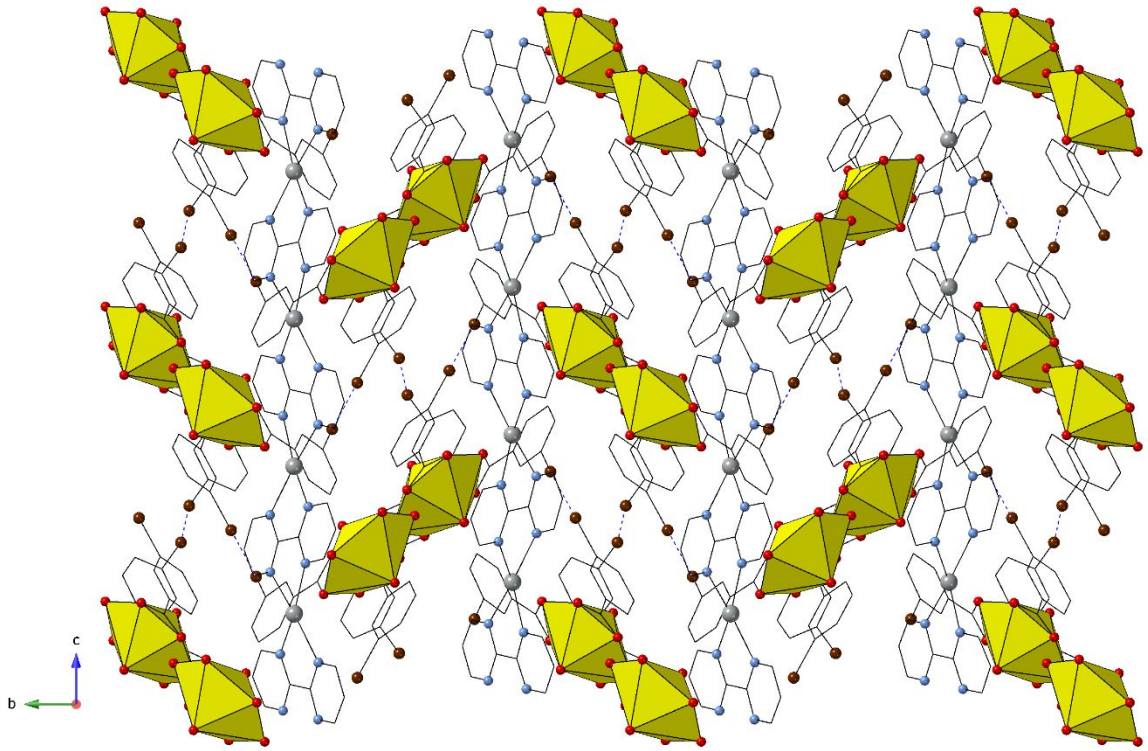

Figure 16. Global structure of compound **8**. Halogen bonding between Br atoms on adjacent 3-bromobenzoate ligands is depicted by the dotted blue lines.

Compound **9**, [Ag(bypm)][UO_2(3-ClBA)$_3$], is isomorphous to compound **8** with only difference being the orientation of the halogens. Despite the differences in the halogens, the two compounds experience similar packing. The UO_2^{2+} cation has U=O bond lengths of 1.770(3) (O1) Å and 1.759(3) Å (O2) an ∠O-U-O of 178.9(1)° (Figure 17). The Ag-O distance is 3.359(3) Å and has a ∠U-O-Ag of 170.7(2)°. (Global structure Figure 18).

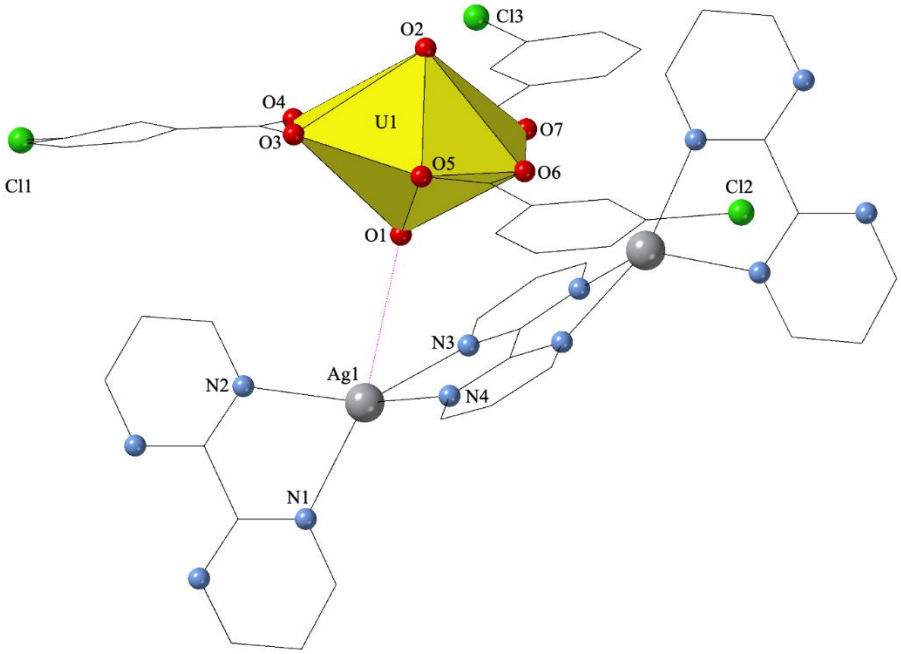

Figure 17. Local representation of compound **9** detailing the metal coordination environments.

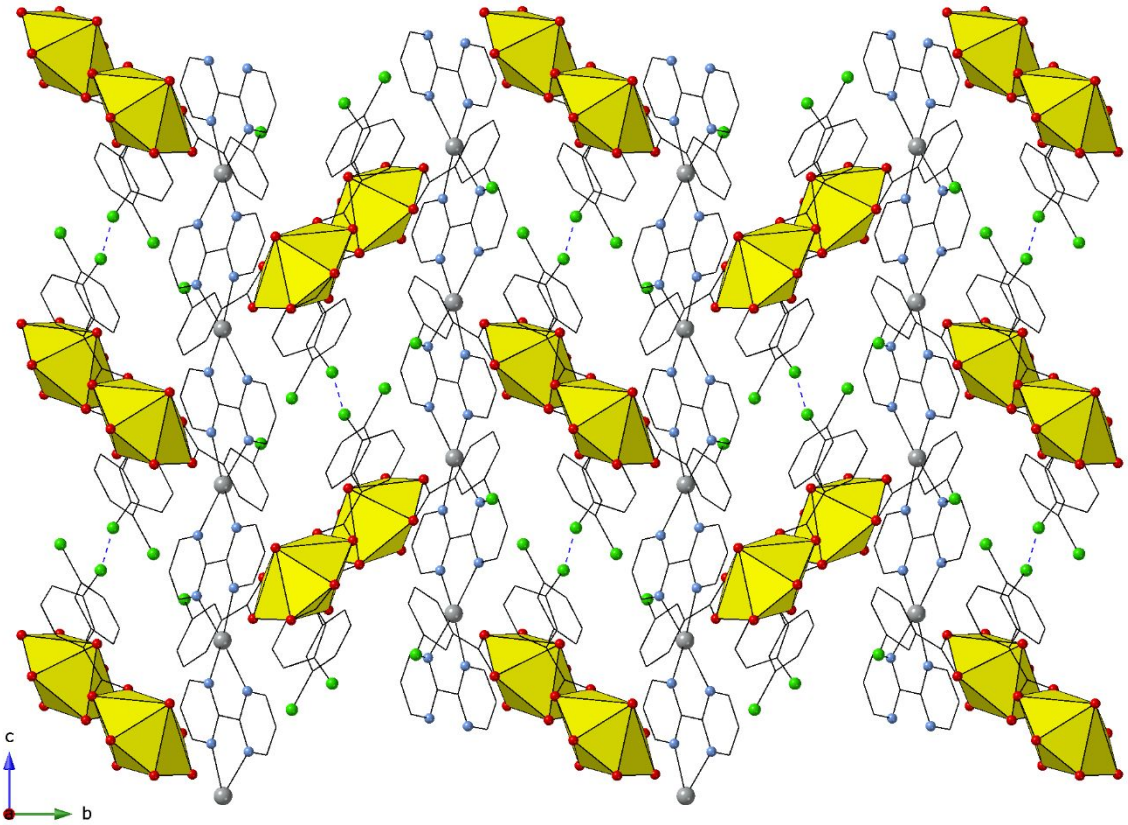

Figure 18. Global structure of compound **9**. Halogen bonding between Cl atoms on adjacent 3-chlorobenzoate ligands is depicted by the dotted blue lines.

Compound **10**, $[Ag_2(bypm)]_2[UO_2(4\text{-}FBA)_2NO_3]$, crystallizes in the space group *Pccn* and the asymmetric unit contains a single crystallographically unique UO_2^{2+} cation, adopting a hexagonal bipyramidal geometry, as well as three crystallographically unique four-coordinate Ag^+ cations (Figure 19). The UO_2^{2+} cation is coordinated in the equatorial plane by two bidentate 4-fluorobenzoate ligands and one bidentate nitrate molecule forming a monomeric unit. The axial U=O bonds have bond lengths of 1.778(2) Å (O1) and 1.767(2) Å (O2) with a ∠O-U-O of 178.5(1)°. Each unique Ag^+ cations forms a bidentate coordination with two 2,2'-bipyrimidine ligands. The 2,2'-bipyrimidine ligands each coordinate to additional Ag^+ cations, forming three crystallographically unique 1-dimensional chains in the [001] direction. There is also lattice nitrate anion and a lattice water molecule (O13) which form hydrogen bonds *via* H2 and O11 on the nitrate anion and H1 and O10 on another nitrate anion. The UO_2^{2+} monomer and the Ag^+ chains containing Ag3 are assembled *via* π-π interactions between the 2,2'-bipyrimidine ligand coordinated to the Ag^+ and a 4-fluorobenzoate ligand coordinated to the UO_2^{2+} (Figure 20). The Ag-O distance is 3.518(2) Å and the ∠U-O-Ag is 113.52(8)°.

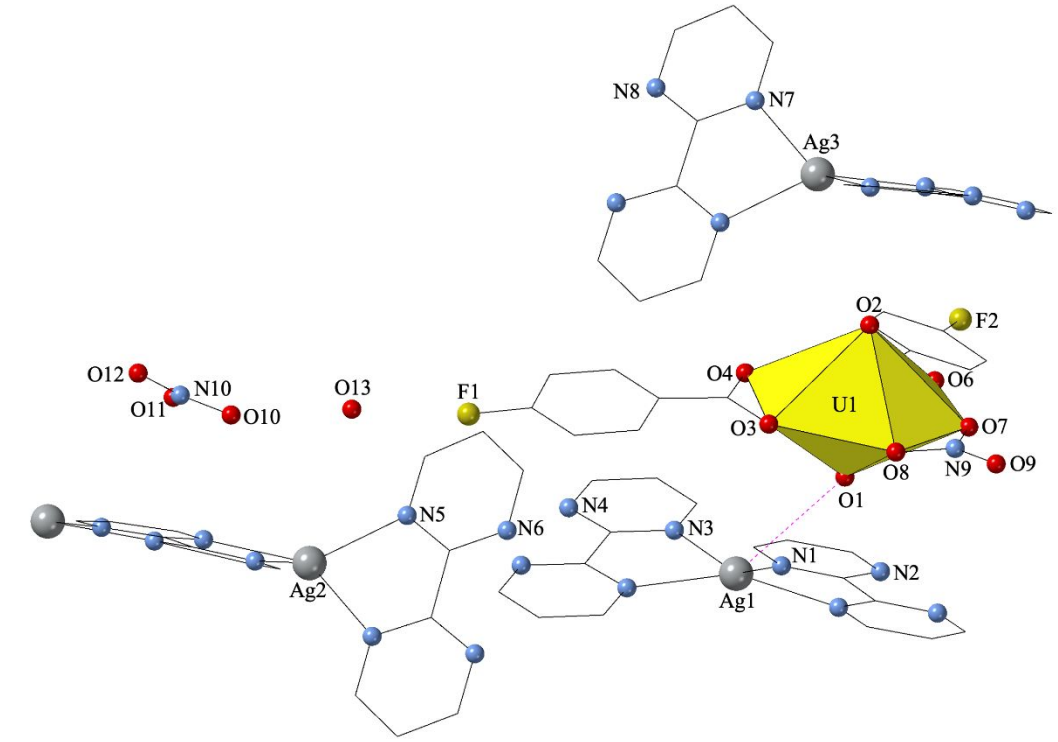

Figure 19. Local representation of compound **10** detailing the metal coordination environments.

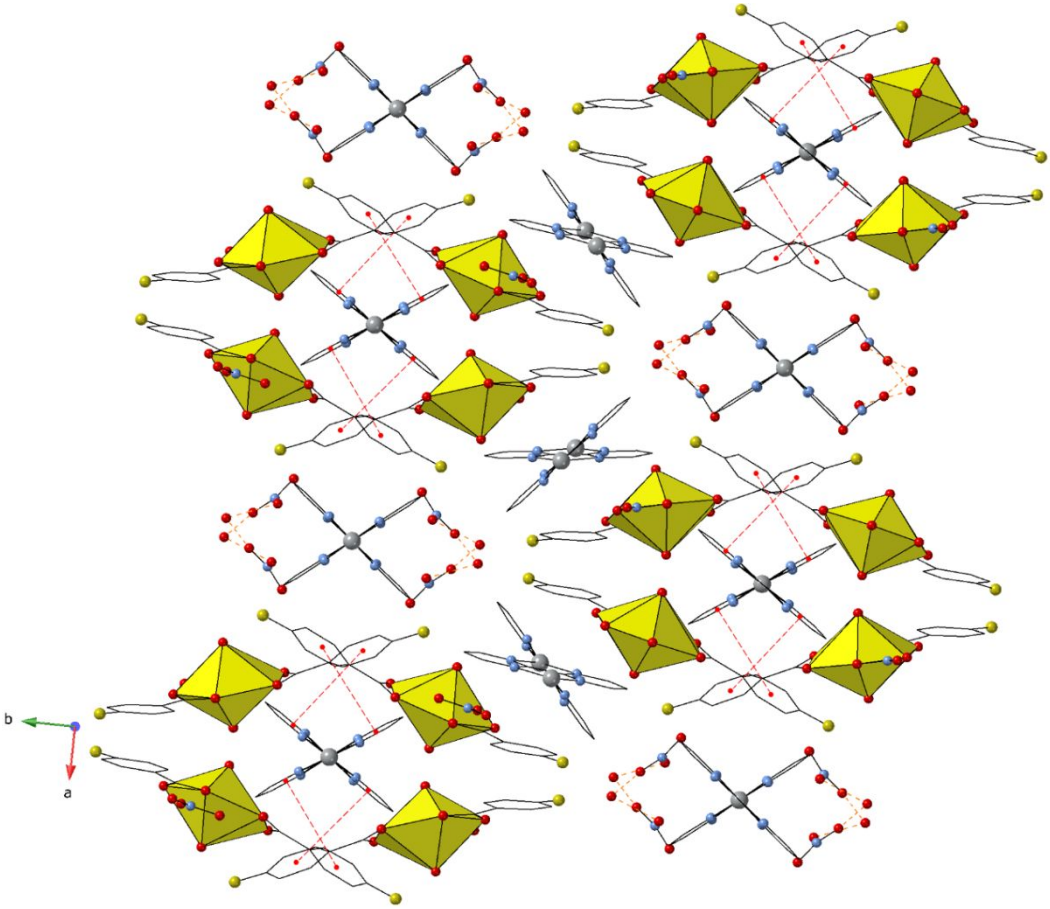

Figure 20. Global structure of compound **10**. Hydrogen bonding between water molecules and nitrate oxygen atoms is depicted by the dotted orange lines. π-π interactions between 4-fluorobenzoate and 2,2'-bipyrimidine centroids are depicted by red dotted lines.

Compound **11**, [Ag(bypm)][UO_2(3-FBA)(Ox)], crystallizes in the space group *P-1* and the asymmetric unit contains a single crystallographically unique UO_2^{2+} cation adopting a pentagonal bipyramidal geometry as well as one crystallographically unique four-coordinate Ag^+ cation (Figure 21). The UO_2^{2+} cation is coordinated in the equatorial plane by two crystallographically equivalent bidentate oxalate ligands (*via* O1 and O2) and by one monodentate 2,5-dichlorobenzoate ligand. The oxalate ligands bridge UO_2^{2+} cations to form 1-dimensional chains along the [010] direction. The axial U=O bonds have bond lengths of 1.771(3) Å (O1) and 1.770(3) Å (O2) with a ∠O-U-O of 177.1(1)°. The Ag^+ cation forms a bidentate coordination with two 2,2'-bipyrimidine ligands *via* N1, N2, N3 and N4. The 2,2'-bipyrimidine ligands each coordinate to other Ag^+ cations, forming 1-dimensional chains in the [001] direction (Figure 22). There are also π-π interactions between the 2,2'-bipyrimidine ligands coordinated to the Ag^+ cations and the 3-fluorobenzoate ligands on the UO_2^{2+} cations. The Ag-O distance is 4.070(7) Å and the ∠U-O-Ag is 156.0(1)°.

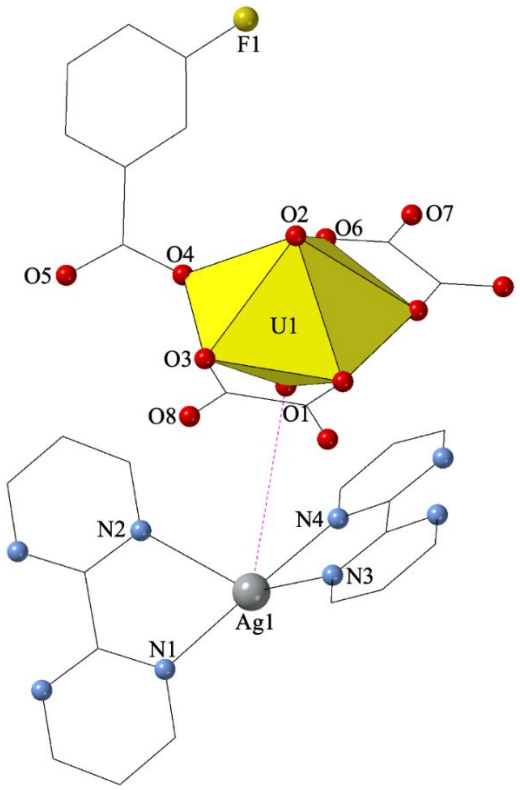

Figure 21. Local representation of compound **11** detailing the metal coordination environments.

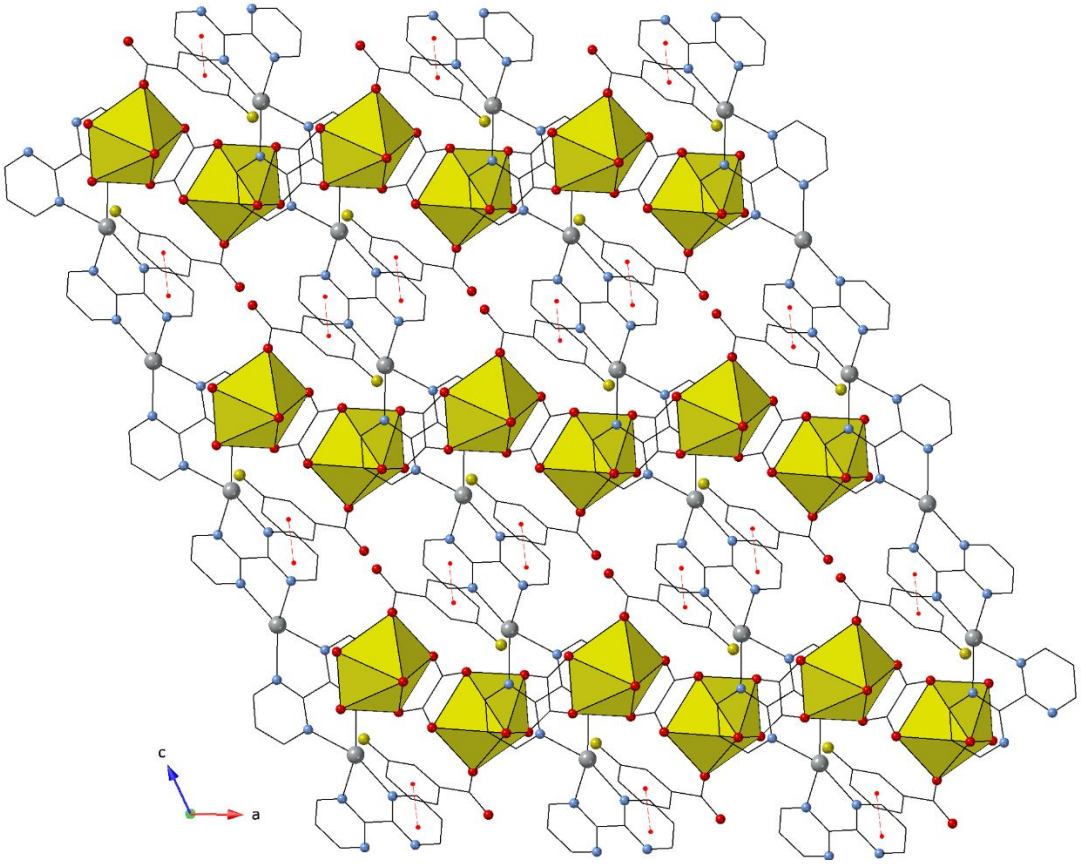

Figure 22. Global structure of compound **11**. π-π interactions between 3-fluorobenzoate and 2,2'-bipyrimidine centroids are depicted by red dotted lines.

Compound **12**, $[UO_2Ag(bypm)_{0.5}(3,5\text{-diClBA})_3]$, crystallizes in the space group *P-1* and the asymmetric unit contains a single crystallographically unique UO_2^{2+} cation adopting a pentagonal bipyramidal geometry as well as one crystallographically unique three-coordinate Ag^+ cation (Figure 23). The UO_2^{2+} cation is coordinated in the equatorial plane by one bidentate 3,5-dichlorobenzoate ligand (*via* O3 and O4) and three monodentate 3,5-dichlorobenzoate ligand (*via* O5 and O7). Two of the 3,5-dicholobenzoate ligands are crystallographically equivalent and serve to bridge to another UO_2^{2+} cation *via* the carboxylate group containing O7 and O8. The axial U=O bonds have bond lengths of 1.772(2) Å (O1) and 1.770(2) Å (O2) with a ∠O-U-O of 178.4(1)°. The Ag^+ cation forms a bidentate coordination with one 2,2'-bipyrimidine ligand *via* N1, and N2. Additionally, the Ag^+ is bridged to the UO_2^{2+} unit through the carboxylate group of a 3,5-dicholobenzoate ligand containing O5 and O6, forming doublewide chains alternating UO_2^{2+} and Ag^+ cations in the [100] direction. These chains are assembled *via* halogen bond interactions between chlorine atoms on 3,5-dichlorobenzoate ligands in adjacent chains (Figure 24). The Ag-oxo distance is 4.287(4) Å with a ∠U-O-Ag of 83.8(1)°.

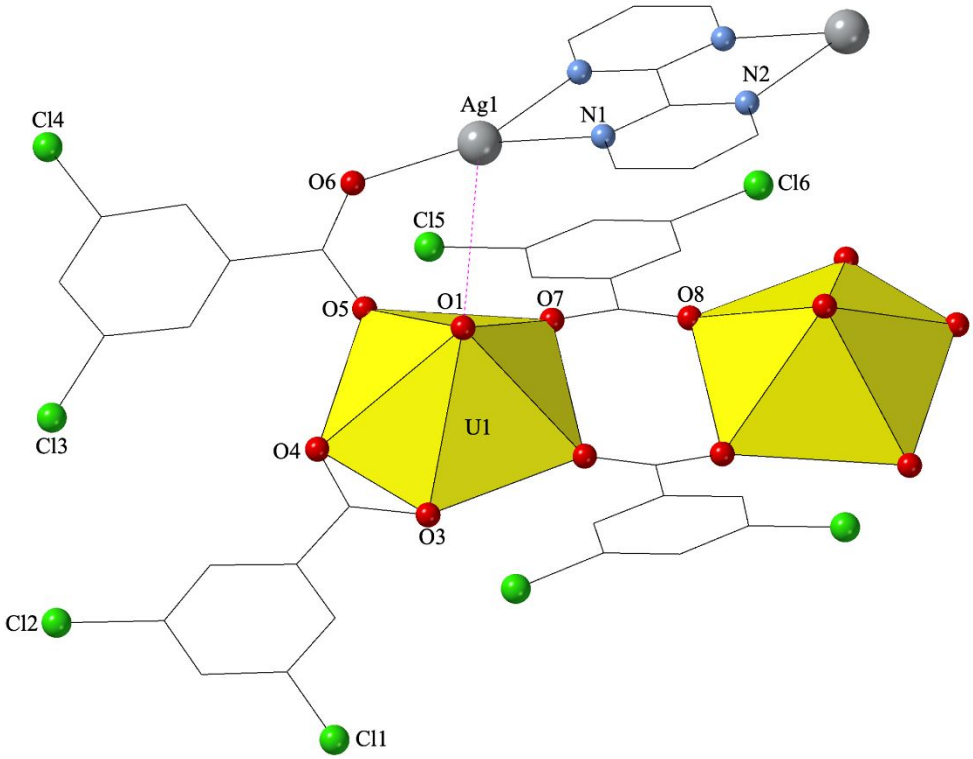

Figure 23. Local representation of compound **12** detailing the metal coordination environments.

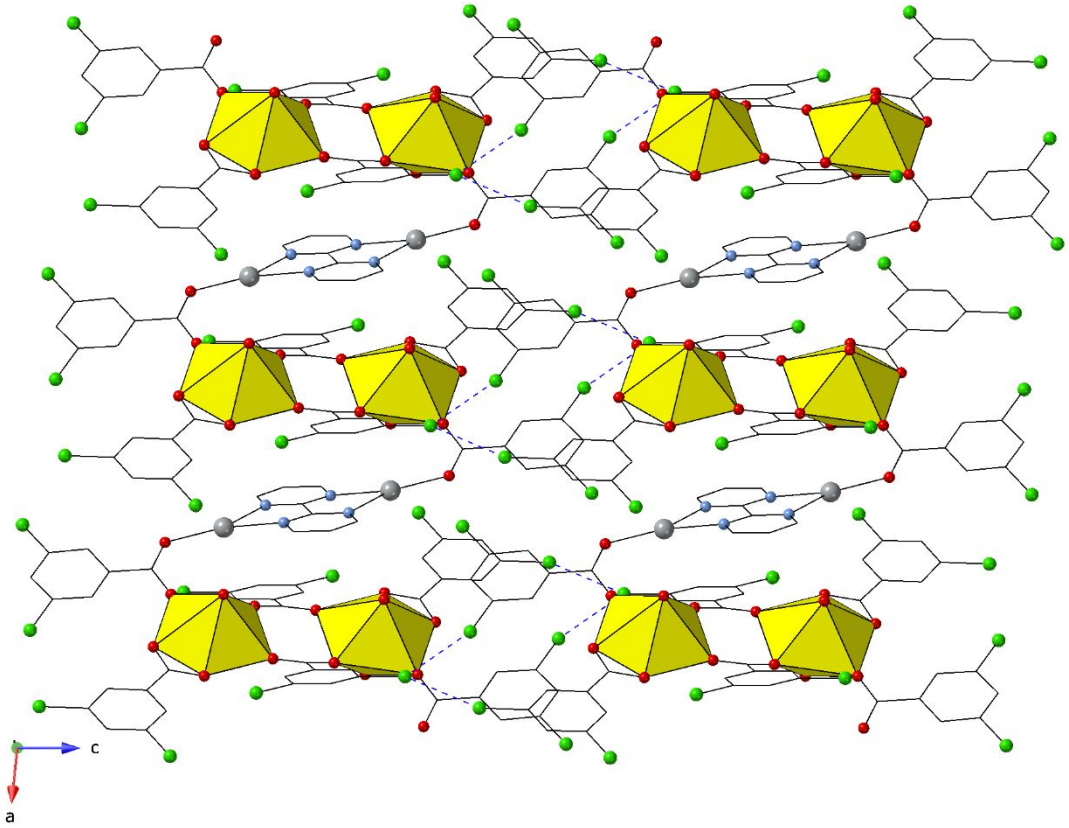

Figure 24. Global structure of compound **12**. Halogen bonding between Cl atoms on adjacent 3,5-dichlorobenzoate ligands is depicted by the dotted blue lines.

Ag^+ Interactions with Uranyl Oxo atoms. Interaction between closed-shell Pb^{2+} cations and the UO_2^{2+} cation have been investigated by our group in the past to study the effects on bonding and photophysical properties of the uranyl cation.[17] It was found that crystallographically determined Pb-oxo distances served as an indication of the strength of the interaction, with shorter distances leading to stronger interactions between the metal and uranyl cations. Here we use the same indicator in order to study the effects of the closed-shell Ag^+ cation on U=O bonds. We have tabulated the shortest Ag-oxo distances in compounds **1-12** in Table 3. These compounds display a range of values from 2.475(3) Å to 4.287(4) Å which all fall within the range of Ag-oxo distances reported in the CSD.[27]

A commonly used crystallographic metric when evaluating the strength of an interaction is the sum of the van der Waals radii (vdW) of the two interacting atoms; this is equal to 3.24 Å for a Ag-O interaction (Ag radius: 1.72 Å and O radius: 1.52 Å).[50] This value is generally presented as a percentage of their overlap and is commonly used to look at non-covalent interactions such as halogen bonds where it serves as a relative measure of the strength of the interaction. Generally, an interaction falling within 100% of the sum of the van der Waals indicates a significant interaction and values >100% indicate a weaker or no interaction. The Ag-O %vdW are also tabulated in Table 3 and the values range from 76% to 132% with **1-7** having values that fall within the sum of the vdW and **8-12** displaying values >100%.

Previous work by Arnold et. al. has shown that close interaction of a metal cation with the uranyl oxo group can lead to U=O bond asymmetry, and in extreme cases even cause reduction of U(VI) to U(V).[3,4,12] However, these effects on bonding decrease with more polarizable metals. There is no evidence of significant bond asymmetry in most of **1-12,** indicating that Ag^+ does not have a substantive effect on strength of the U=O bonds as compared to Pb^{2+} in our previously reported Pb^{2+}/UO_2^{2+} complexes,[17] as well as the heterometallic complexes reported by Arnold et al. This is in agreement with Arnold et. al.'s conclusion that more polarizable metals do not have a strong an effect on the uranyl cation.[3,4,12] It is of note however that compound **1** which has the shortest Ag-O interaction distances has the highest degree of bond asymmetry with a difference in U=O bond lengths of 0.02 Å.

Table 3. Summary of crystallographically determined Ag-oxo interaction parameters.

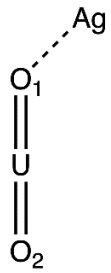

Compound	Ag···O1	%vdW	U=O1 (Å)	U=O2 (Å)	Ag···O1=U (deg)
1	2.475(3) Å	76%	1.781(3)	1.761(3) Å	127.0(2) Å
2	2.645(3) Å	82%	1.767(2)	1.767(2) Å	137.1(2) Å
3	2.647(3) Å	82%	1.773(1)	1.773(1) Å	135.9(1) Å
4	2.742(2) Å	85%	1.772(2)	1.778(2) Å	140.7(1) Å
5	2.875(2) Å	89%	1.776(3)	1.773(3) Å	115.1(1) Å
6	2.932(7) Å	90%	1.769(6)	1.773(5) Å	141.7(3) Å
7	3.093(4) Å	95%	1.769(4)	1.771(4) Å	143.0(2) Å
8	3.314(6) Å	102%	1.766(5)	1.752(5) Å	171.8(3) Å
9	3.359(3) Å	104%	1.770(3)	1.759(3) Å	170.7(2) Å
10	3.518(2) Å	109%	1.778(2)	1.767(2) Å	113.5(1) Å
11	4.070(3) Å	126%	1.771(3)	1.770(3) Å	156.0(1) Å
12	4.287(4) Å	132%	1.772(2)	1.770(2) Å	83.8(1) Å

Spectroscopic Properties.

It is well-known that interaction with the uranyl unit, whether in the equatorial plane or at the axial oxo groups, can lead to changes in the bonding construct of the cation, which in turn lead to changes in the electronic structure of the compound.[3,5,6,12,13,51–53] In order to investigate these changes, we used luminescence and Raman spectroscopy to study the electronic structure of the uranyl cation in these compounds.

Uranyl-containing compounds typically display a bright green luminescence signature. Generally, the emission band ranges from 450 nm to 650 nm and has five or more finger-like peaks while the excitation profile features two bands centered around 420 nm and 340 nm. The unique excitation profile occurs due to an electronic transition between uranium 5f δ_u and ϕ_u orbitals and the ground state uranyl bonding orbitals ($3\sigma_u$, $3\sigma_g$, $1\pi_g$, $2\pi_u$) and vibronic coupling with the 855cm^{-1} U=O symmetric stretch results in the vibrationally resolved peaks.[54] Compounds **3-6** and **8-12** all display the characteristic emission peaks and two excitation bands while the luminescence signatures for **1**, **2**, and **7** are quenched.

We had noted previously that Pb^{2+} cations are able to quench uranyl luminescence in compounds with Pb-oxo contacts at 87% of the vdW or lower.[17] In the Ag^+ containing compounds reported herein, we note that **1** and **2** (vdW% of 75% and 82% respectively), which feature the closest Ag-oxo distances, do not display any uranyl emission. That said, compounds **3** and **4** do not display any noticeable quenching despite having vdW% of 82% and 85% respectively. This suggests that compared the Pb-oxo interactions, the Ag^+ cation requires much closer interactions to be able to induce quenching. It is of note that **7** displays reduced emission despite having a longer Ag-O interaction. As such it is unlikely that this quenching occurs as a result of interaction with the Ag^+ cation, this suggests that another quenching mechanism may be at play.

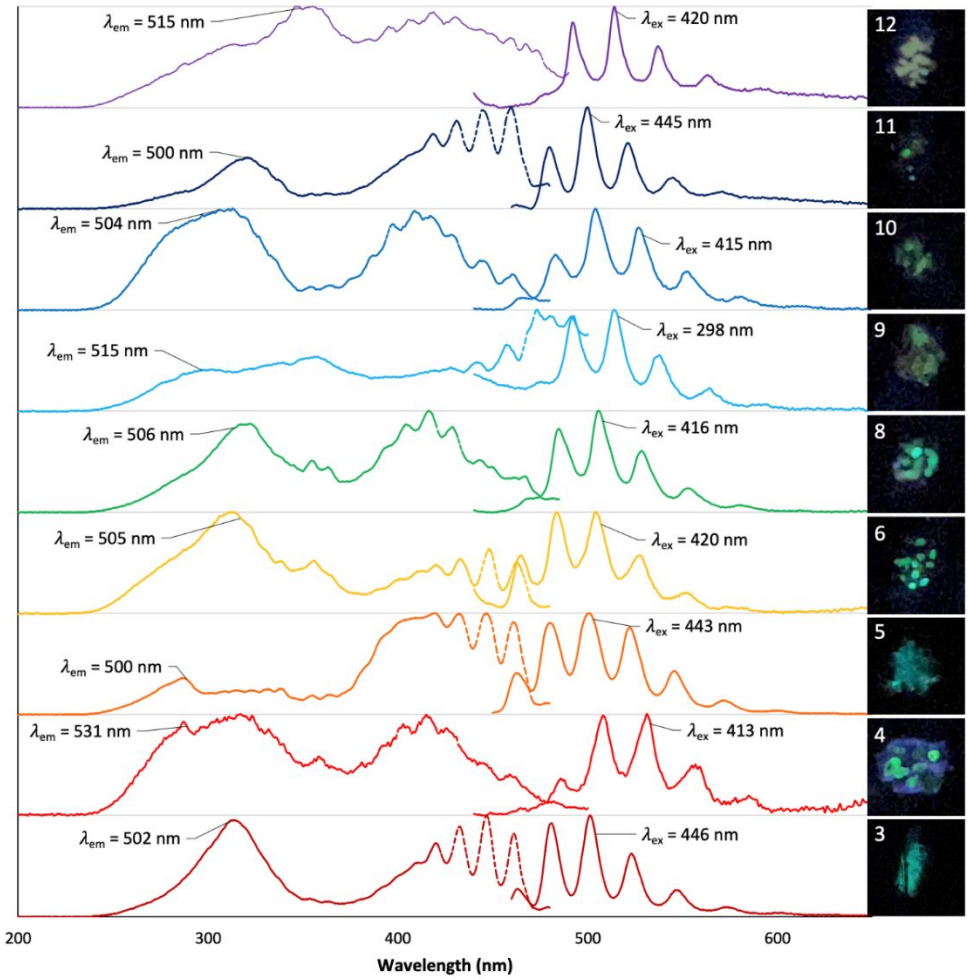

Figure 25. Luminescence spectra of compounds **3-6, 8-12** at 298K with photoimages under a 340 nm UV light. **1, 2,** and **7** did not display luminescence signatures.

Raman spectroscopy. The uranyl cation has three vibrational modes: the symmetric stretch (v_1, Raman active), the asymmetric bend (v_2, IR active), and the asymmetric stretch (v_3, IR active). The Raman active symmetric stretch is the mode of interest as it is generally more easily identifiable and is sensitive both to coordination in the equatorial plane of the uranyl cation and also to interaction at the –yl oxo groups. Both equatorial coordination and axial interactions have a tendency to lead to red-shifting of the U=O symmetric stretch peak, corresponding to weakening of the bond. Generally, values for this peak are observed in the 860-880 cm^{-1} region but have been observed across the range of 900 to 750 cm^{-1}.[51]

The Raman spectra for compounds **1-12** are reported in Figure 26. All compounds display peaks in the 800-900 cm^{-1} region. Compounds **1, 6, 7** and **10-12** display only one sharp peak in this region which we attribute to the U=O symmetric stretch with values of 829 cm^{-1}, 837 cm^{-1}, 838 cm^{-1}, 830 cm^{-1}, 838 cm^{-1}, 870 cm^{-1}, 843 cm^{-1}, and 840 cm^{-1}, respectively. Compounds **2** and **3** both display peaks at 839 cm^{-1} and 838 cm^{-1} with notable shoulders. These shoulders likely occur as a result of two crystallographically unique uranyl centers in each compound which have different U=O bond

lengths. In **2,** the uranyl cation interacting closely with the Ag^+ cation has equivalent U=O bond lengths of 1.767(2) Å while the UO_2^{2+} cation that is not interacting closely with the Ag^+ has U=O bond lengths of 1.774(3) and 1.760(3) Å. In **3,** the U=O center interacting closely with the Ag^+ cation has equivalent U=O bond lengths of 1.773(1) Å and the U=O cation that is not interacting closely with the silver has bond lengths of 1.774(3) and 1.763(3) Å. The overlap of the U=O symmetric stretch peaks corresponding to each of these different cations would explain the presence of the shoulders. Compound **4** also displays two peaks despite not having a secondary metal center but the peak at 850 cm^{-1} has been attributed to the 4-fluorobenzoate ligand in the structure.[55] As such we can attribute the remaining peak at 870 cm^{-1} to the U=O symmetric stretch. Compounds **5** displays two peaks in the 800-900 cm^{-1} range at 833 and 851 cm^{-1}. While this compound does have two crystallographically inequivalent uranyl centers, the bond lengths of these centers (1.776(3), 1.772(3) Å and 1.776(3), 1.773(3) Å) are very similar and therefore we would not expect such a large difference in the energy of the symmetric stretches corresponding to these uranyl units. A comparison of the above peak values with the Raman spectra of the organic ligands in the structure did not match either of the values of the peaks. As such, we have not been able to accurately assign the U=O symmetric stretch for this complex and this spectrum has been excluded from the analysis.

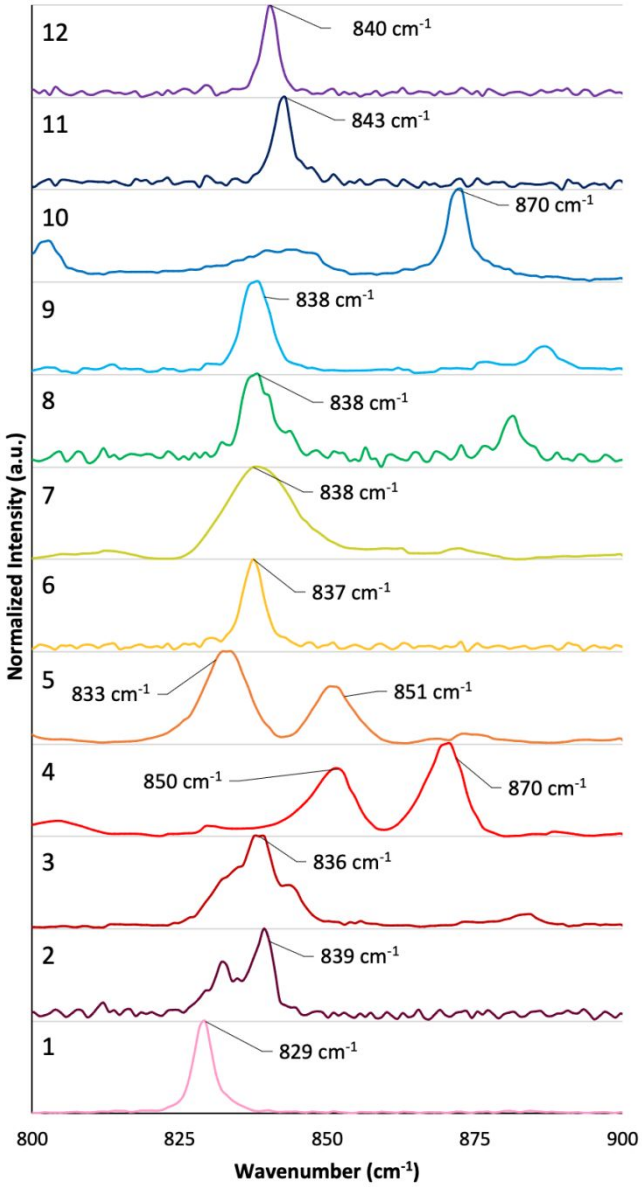

Figure 26. Raman spectra of compounds **1-12** at 298 K.

Previous work done by our group and others have reported that close interaction of metal cations at the oxo group can lead to shifting of the Raman U=O symmetric stretch values.[13,52–54] Overall we do not observe such a trend of Raman red-shifting with Ag-oxo distance, though it is worth noting that compound **1,** which experiences the closest Ag-oxo interaction, does have the most red-shifted symmetric stretch peak by 7 cm^{-1} as compared to the next lowest energy peak value in compound **3**. This red-shifting indicates a bond weakening in this compound as compared to the other compounds and is supported by the higher bond asymmetry displayed by **1** as compared to the other compounds. Additionally, compound **1** displays quenched luminescence which suggests the Ag^{+} cation only has significant effects on the bonding and photophysical properties of this compound with contacts at <80% of the %vdW.

Characterizing Uranyl Second Sphere Interactions and Inner Sphere Bonding

Second Sphere Interactions. Whereas the Raman and luminescence spectroscopy can give insight on the U=O bonds, the second-sphere interactions between the Ag^+ and the uranyl-oxo group require second order perturbation theory based (SOPT) NBO calculations. These calculations determine orbital pairs and provide an additional stabilization energy in kcal/mol afforded to the structure as a result of these interactions as a function of the orbital overlap and energy difference as described in Equation 1.

$$E(2) = \Delta E_{ij} = q_i \frac{F(i,j)^2}{\varepsilon_j - \varepsilon_i} \quad (1)$$

Four different types of donor/acceptor orbital pair interactions between orbitals on the Ag^+ cation and the uranyl unit were determined by SOPT for each M-oxo interaction (Figure 27). The four types are: 1) electron donor Ag *s* valence orbital and an acceptor empty U *5f* orbital, (2) a donor Ag *s* valence orbital and a UO_2 σ* antibonding orbital acceptor, (3) a donor O sp^x lone pair and an empty acceptor Ag *d* orbital, and (4) a donor UO_2 σ bonding orbital and an empty acceptor Ag *d* orbital.

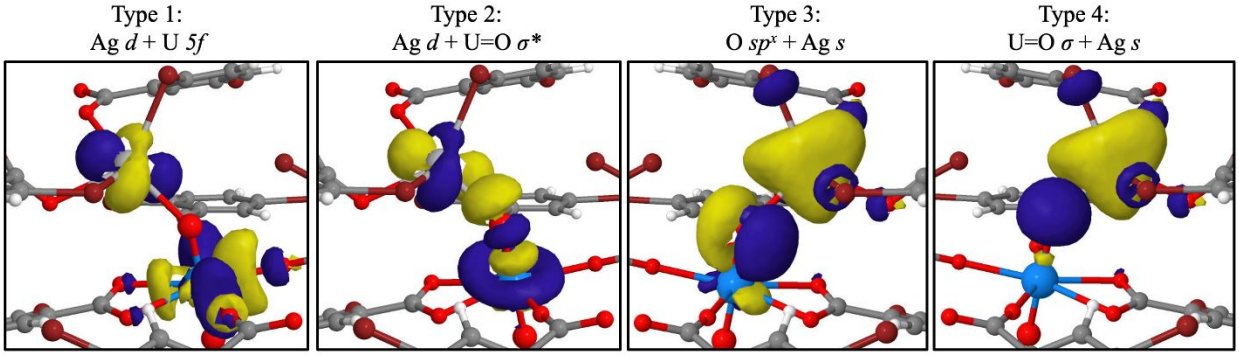

Figure 27. Isodensity renderings of representative orbitals involved in Ag-oxo interactions using compound **1** as a model.

Each of these four types of interactions has a stabilization energy calculated in kcal/mol where higher energy values are indicative of a stronger interaction. These values for **1-12** are tabulated in Table 4. In all compounds, the highest stabilization energy corresponds to the Type 3 interaction between the oxo group lone pair electrons and the empty Ag *d* orbitals. This likely due to the closer proximity of the orbital centered on the oxo group and the silver leading to more orbital overlap. The Type 4 and Type 2 interactions are generally similar in strength. These interactions are of note as they involve donation into U=O σ* anti-bonding orbitals and out of U=O σ bonding orbitals. This would suggest that strong interactions between these orbital pairs would lead to a subsequent weakening of the U=O bond. The relatively low stabilization energy values of Types 2 and 4 would explain why this U=O bond weakening is not seen in the structural or spectroscopic data for most compounds. Only **1** which has a Type 4 interaction strength of 2.01 kcal/mol and a Type 2 interaction strength of 0.98 kcal/mol (which are double almost all other values for these orbital interaction types in the other compounds herein) shows changes in the spectroscopy and bonding.

Table 4. Second Order Perturbation Theory calculated NCI stabilization energies (kcal mol^{-1}) and orbitals involved in charge transfer.

		$Ag^+ \rightarrow UO_2^{2+}$		$UO_2^{2+} \rightarrow Ag^+$		
	Ag-O Distance	**Type 1 Ag *d* → U *5f* (kcal/mol)**	**Type 2 Ag d → UO_2 σ* (kcal/mol)**	**Type 3 O sp^x → Ag s (kcal/mol)**	**Type 4 UO_2 σ → Ag s (kcal/mol)**	**Total (kcal/mol)**
1	2.475 Å	0.64	0.98	7.40	2.01	11.03
2	2.645 Å	0.06	0.18	5.37	0.88	6.49
3	2.647 Å	0.12	0.41	6.04	0.48	7.05
4	2.742 Å	0.00	0.31	5.79	0.28	6.38
5	2.875 Å	0.19	0.47	4.61	1.59	6.86
6	2.932 Å	0.00	0.22	3.62	0.20	4.04
7	3.093 Å	0.00	0.13	2.43	0.12	2.68
8	3.314 Å	0.00	0.11	0.96	0.07	1.14
9	3.359 Å	0.00	0.11	0.86	0.06	1.03
10	3.518 Å	0.06	0.00	1.01	0.00	1.07
11	4.070 Å	0.00	0.00	0.13	0.00	0.13
12	4.287 Å	0.06	0.00	0.18	0.10	0.34

By combining the values of the four different interaction types we can determine the *overall* strength of the interaction between the Ag^+ cation and the uranyl-oxo group. When plotting these combined values against the Ag-oxo distance (Figure 28), we see that the stabilization energy value increases exponentially with decreasing Ag-oxo distance. The highest stabilization energy (compound **1**) is 11.03 kcal/mol after which there is a sharp decrease in compound **2** to 6.49 kcal/mol.

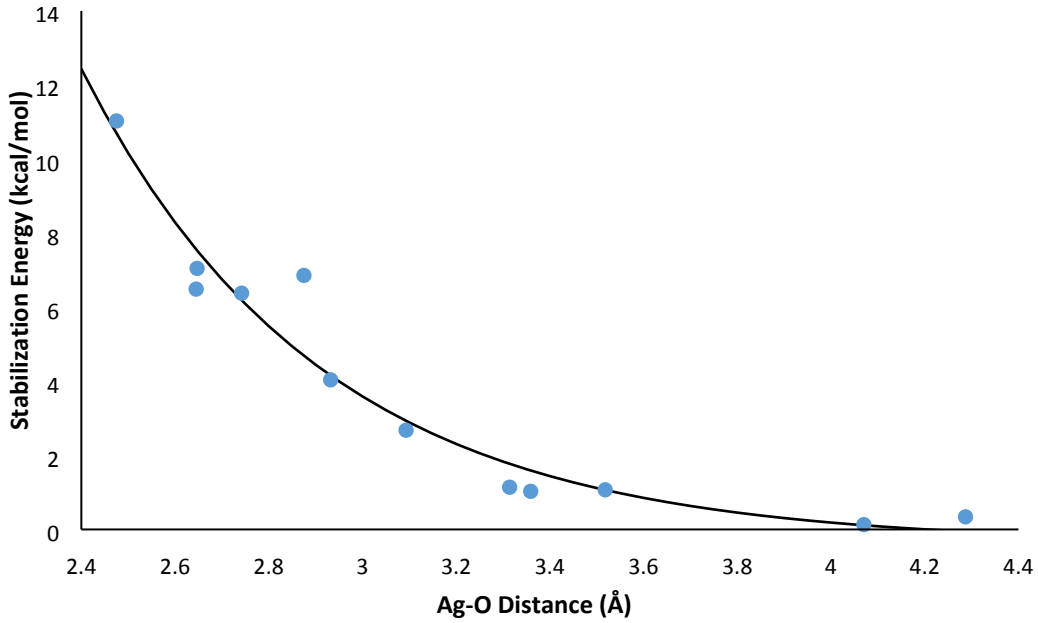

Figure 28. First-order exponential fit of Ag-oxo distance versus total uranyl-cation interaction stabilization energy highlighting the relationship between distance and interaction strength between the UO_2^{2+} and the Ag^+ units.

Inner Sphere U=O Bonding. We use Quantum Theory of Atoms in Molecues (QTAIM) to determine bond critical points (BCP) between close atom pairs and calculate their electron densities which we then use to measure the strength and covalency of these bonds. Higher electron density values indicate a stronger, more covalent bond. We summarize the electron density (ρ) values as calculated by QTAIM for the Ag-O interactions and the U=O bonds in the interacting uranyl cation for **1-12** in Table 5. The highest Ag-O electron density value is 0.034 in **1** which displays the closest Ag-O contact. As with the stabilization energy values, the bond critical point electron densities display an exponential increase with decreasing Ag-O distance (Figure S23). Additionally, there is a linear correlation between the Ag-O bond critical point electron density and the total stabilization energy calculated with SOPT (Figure S24).

Table 5. Quantum Theory of Atom in Molecules calculated bond critical point electron densities (ρ)

	Ag-O	U=O (Ag)	U=O
1	0.034	0.297	0.314
2	0.024	0.307	0.311
3	0.023	0.303	0.307
4	0.020	0.301	0.302
5	0.016	0.301	0.305
6	0.014	0.304	0.305
7	0.010	0.304	0.307

8	0.007	0.309	0.322
9	0.006	0.306	0.316
10	0.000	0.300	0.311
11	0.000	0.303	0.307
12	0.000	0.306	0.308

Similar treatment of UO_2^{2+}/Pb^{2+} has demonstrated that close Pb-oxo interactions lead to a relative *decrease* in electron density in the U=O bond as compared to the U=O bond not interacting with the metal, resulting in bond asymmetry.[17] In these Ag-containing compounds we do not see a similar trend with the exception of **1** where the Ag-interacting U=O bond has a BCP electron density values of 0.297 while the other U=O bond has a value of 0.314. The asymmetry and lower BCP electron density value displayed by compound **1** is supported by the structural data, which has the highest bond asymmetry with a difference of 0.02 Å between U=O bond lengths displayed in the structural data. The increased effect of Ag^+ on the U=O bonds in this compound is supported by the significantly higher stabilization energy calculated for this interaction by SOPT as compared to the other compounds with longer Ag-oxo interactions. The effects of this stronger interaction and increased bond asymmetry are also supported by the spectroscopy where compound **1** displays the most red-shifted U=O symmetric stretch value, as well as quenched luminescence emission.

One additional observation of interest is the relationship between the M-oxo stabilization energy and the BCP electron density value in the Ag/UO_2^{2+} materials as compared to the previously reported Pb/UO_2^{2+} materials. In both groups of compounds there is a linear correlation between increasing stabilization energy and BCP electron density. Of interest, however, is that, at similar %vdW values, the Ag-oxo interactions have lower stabilization energies as compared to Pb-oxo interactions, but the BCP electron density values at those %vdW are *higher* for the Ag-oxo interactions. For the Pb-oxo interaction, the highest BCP electron density value was 0.020 corresponding to an interaction distance of 2.812 Å (80% VdW) and a stabilization energy of 17.05 kcal/mol.[17] For the silver-containing compounds, **1-3** all have higher Ag-O BCP electron densities despite the much lower stabilization energies (11.03, 6.49, and 7.05 kcal/mol respectively) and similar vdW values (76%, 82%, and 82% respectively). The markedly higher electron density within these bonds suggests that despite the weaker interactions, there is still more electron density being shared in the interaction as compared to the Pb-containing compounds. This suggests that the Ag-oxo interaction is more covalent in nature as compared to the Pb-oxo interaction which, due to higher charge density, may experience a greater electrostatic component of the interaction.

Conclusion

We report the synthesis and characterization of 12 novel Ag^+/UO_2^{2+} heterometallic complexes. Structural data revealed Ag-oxo interactions ranging from 76% to 132% of the sum of the Van der Waals radii for these atoms. Unlike with previously reported Pb^{2+}/UO_2^{2+} materials which displayed the effects of Pb-oxo interactions even at vdW% distances of 87%, only compound **1** (at 76%) displayed quenched luminescence emission, red-shifting in the U=O symmetric stretch, and bond asymmetry displayed both structurally and in the computed BCP

electron density values as a result of the Ag-oxo interaction. This change in behavior was observed through. SOPT analysis revealed that the orbitals with the most significant contribution to the Ag-oxo interaction to be the O sp^x → Ag d but that smaller interactions involving U=O bonding and antibonding orbitals also contributed albeit weakly (U=O σ → Ag d and Ag s → U=O σ*). The overall stabilization energies for these interactions were relatively low though with only **1** displaying a stabilization energy above 8 kcal/mol. The smaller relative energies associated with these interactions is supported by the lack of bond weakening in U=O bonds seen in both the spectroscopy and the structural data **2-12**. We attribute the smaller effects of the Ag^+ on the uranyl cation to its high polarizability. Despite the overall weaker effects of the Ag^+ cation as compared to the Pb^{2+}, comparison of the BCP electron density values calculated with QTAIM indicated that the Ag-oxo interaction has more covalent character than the Pb-oxo interaction. A continued study including other metal cations is underway in order to characterize further trends and lead to a more in-depth understanding of interactions occurring at the terminal uranyl oxo.

Associated Content

Electronic Supplementary Information

The Electronic Supplementary Information is available XXXX. Crystallographic information on CCDC 2160088-2160099 can be obtained free of charge by e-mailing data_request@ccdc.cam.ac.uk or by contacting The Cambridge Crystallographic Data Centre, 12 Union Road, Cambridge, CB2 1EZ UK; Fax +44(0)1223-336033; http://www.ccdc.cam.ac.uk/data_reque st/cif.

PXRD, additional QTAIM data, DFT models (pdf)
X-ray data for compound **1** (CIF)
X-ray data for compound **2** (CIF)
X-ray data for compound **3** (CIF)
X-ray data for compound **4** (CIF)
X-ray data for compound **5** (CIF)
X-ray data for compound **6** (CIF)
X-ray data for compound **7** (CIF)
X-ray data for compound **8** (CIF)
X-ray data for compound **9** (CIF)
X-ray data for compound **10** (CIF)
X-ray data for compound **11** (CIF)
X-ray data for compound **12** (CIF)

Author Information

***Christopher L. Cahill** - Department of Chemistry, The George Washington University, Washington, DC 20052, United States; orcid.org/0000-0002-2015-3595;
Email: cahill@gwu.edu

Authors

Dominique M. Brager - Department of Chemistry, The George Washington University, Washington, DC 20052, United States; orcid.org/0000-0003-0694-0805;
Email: dbrager@gwu.edu

Alexander C. Marwitz - Department of Chemistry, Georgetown University, Washington, DC 20057, United States; orcid.org/0000-0002-2560-9184;
Email: acm298@georgetown.edu

Author Contributions
The manuscript was written with contributions from all authors.

Notes
The authors declare no competing financial interests.

Acknowledgment
This study was supported by the U.S. Department of Energy (DOE) – Chemical Sciences, Geosciences, and Biosciences Division, Office of Science, Office of Basic Energy Sciences, Heavy Elements Program, under grant number DE-FG02-05ER15736. The authors would like to thank Professor Karah Knope and Anamar Blanes of Georgetown University for providing Raman microscope time. We would also like to thank Professor Raymond Butcher of Howard University for his help with structural refinement of Compound **6**.

References

(1) Arnold, P. L.; Love, J. B.; Patel, D. Pentavalent Uranyl Complexes. *Coord. Chem. Rev.* **2009**, *253* (15–16), 1973–1978. https://doi.org/10.1016/j.ccr.2009.03.014.

(2) Zachara, J. M.; Long, P. E.; Bargar, J.; Davis, J. A.; Fox, P.; Fredrickson, J. K.; Freshley, M. D.; Konopka, A. E.; Liu, C.; McKinley, J. P.; Rockhold, M. L.; Williams, K. H.; Yabusaki, S. B. Persistence of Uranium Groundwater Plumes: Contrasting Mechanisms at Two DOE Sites in the Groundwater–River Interaction Zone. *J. Contam. Hydrol.* **2013**, *147*, 45–72. https://doi.org/10.1016/j.jconhyd.2013.02.001.

(3) Arnold, P. L.; Pécharman, A.-F.; Lord, R. M.; Jones, G. M.; Hollis, E.; Nichol, G. S.; Maron, L.; Fang, J.; Davin, T.; Love, J. B. Control of Oxo-Group Functionalization and Reduction of the Uranyl Ion. *Inorg. Chem.* **2015**, *54* (7), 3702–3710. https://doi.org/10.1021/acs.inorgchem.5b00420.

(4) Arnold, P. L.; Pécharman, A.-F.; Hollis, E.; Yahia, A.; Maron, L.; Parsons, S.; Love, J. B. Uranyl Oxo Activation and Functionalization by Metal Cation Coordination. *Nat. Chem. 2010 212* **2010**, *2* (12), 1056–1061. https://doi.org/10.1038/nchem.904.

(5) Fortier, S.; Hayton, T. W. Oxo Ligand Functionalization in the Uranyl Ion (UO22+). *Coord. Chem. Rev.* **2010**, *254* (3–4), 197–214. https://doi.org/10.1016/j.ccr.2009.06.003.

(6) Carter, K. P.; Kalaj, M.; McNeil, S.; Kerridge, A.; Schofield, M. H.; Ridenour, J. A.; Cahill, C. L. Structural, Spectroscopic, and Computational Evaluations of Cation–Cation and Halogen Bonding Interactions in Heterometallic Uranyl Hybrid Materials. *Inorg. Chem. Front.* **2021**. https://doi.org/10.1039/d0qi01319f.

(7) Yang, W.; Parker, T. G.; Sun, Z. M. Structural Chemistry of Uranium Phosphonates. *Coordination Chemistry Reviews*. Elsevier November 1, 2015, pp 86–109. https://doi.org/10.1016/j.ccr.2015.05.010.

(8) Jayasinghe, A. S.; Payne, M. K.; Forbes, T. Z. Synthesis and Characterization of Heterometallic Uranyl Pyridinedicarboxylate Compounds. *J. Solid State Chem.* **2017**, *254*, 25–31. https://doi.org/10.1016/j.jssc.2017.07.002.

(9) Wang, K. X.; Chen, J. S. Extended Structures and Physicochemical Properties of Uranyl-Organic Compounds. *Acc. Chem. Res.* **2011**, *44* (7), 531–540. https://doi.org/10.1021/ar200042t.

(10) Cahill, C. L.; Lill, D. T. de; Frisch, M. Homo- and Heterometallic Coordination Polymers from the f Elements. *CrystEngComm* **2006**, *9* (1), 15–26. https://doi.org/10.1039/b615696g.

(11) Loiseau, T.; Mihalcea, I.; Henry, N.; Volkringer, C. The Crystal Chemistry of Uranium Carboxylates. *Coordination Chemistry Reviews*. Elsevier May 1, 2014, pp 69–109. https://doi.org/10.1016/j.ccr.2013.08.038.

(12) Arnold, P. L.; Patel, D.; Blake, A. J.; Wilson, C.; Love, J. B. Selective Oxo Functionalization of the Uranyl Ion with 3d Metal Cations. *J. Am. Chem. Soc.* **2006**, *128* (30), 9610–9611. https://doi.org/10.1021/ja0634167.

(13) Bell, N. L.; Arnold, P. L.; Love, J. B. Controlling Uranyl Oxo Group Interactions to Group 14 Elements Using Polypyrrolic Schiff-Base Macrocyclic Ligands. *Dalt. Trans.* **2016**, *45* (40), 15902–15909. https://doi.org/10.1039/c6dt01948j.

(14) Arnold, P. L.; Hollis, E.; White, F. J.; Magnani, N.; Caciuffo, R.; Love, J. B. Single-Electron Uranyl Reduction by a Rare-Earth Cation. *Angew. Chemie Int. Ed.* **2011**, *50* (4), 887–890. https://doi.org/10.1002/anie.201005511.

(15) Arnold, P. L.; Cowie, B. E.; Arkøta Suvova, M.; Zegke, M.; Magnani, N.; Colineau, E.; Griveau, J.-C.; Caciuffo, R.; Love, J. B.; Arnold, P. L.; Owie, B. E. C.; Suvova, M.; Egke, M. Z.; Love, J. B.; Magnani, N.; Colineau, E.; Griveau, J.-C.; Caciuffo, R. Axially Symmetric U−O−Ln- and U−O−U-Containing Molecules from the Control of Uranyl Reduction with Simple f-Block Halides. *Angew. Chemie Int. Ed.* **2017**, *56* (36), 10775–10779. https://doi.org/10.1002/anie.201705197.

(16) Cowie, B. E.; Purkis, J. M.; Austin, J.; Love, J. B.; Arnold, P. L. Thermal and Photochemical Reduction and Functionalization Chemistry of the Uranyl Dication, [UVIO2]2+. *Chem. Rev.* **2019**, *119* (18), 10595–10637. https://doi.org/10.1021/acs.chemrev.9b00048.

(17) Brager, D. M.; Nicholas, A. D.; Schofield, M. H.; Cahill, C. L. Pb-Oxo Interactions in Uranyl Hybrid Materials: A Combined Experimental and Computational Analysis of Bonding and Spectroscopic Properties. *Inorg. Chem.* **2021**, *60* (22), 17186–17200. https://doi.org/10.1021/acs.inorgchem.1c02518.

(18) Zhao, R.; Mei, L.; Hu, K. Q.; Tian, M.; Chai, Z. F.; Shi, W. Q. Bimetallic Uranyl Organic Frameworks Supported by Transition-Metal-Ion-Based Metalloligand Motifs: Synthesis, Structure Diversity, and Luminescence Properties. *Inorg. Chem.* **2018**, *57* (10), 6084–6094. https://doi.org/10.1021/acs.inorgchem.8b00634.

(19) Thuéry, P.; Rivière, E.; Harrowfield, J. Uranyl and Uranyl-3d Block Cation Complexes with 1,3-Adamantanedicarboxylate: Crystal Structures, Luminescence, and Magnetic Properties. *Inorg. Chem.* **2015**, *54* (6), 2838–2850. https://doi.org/10.1021/ic503004j.

(20) Thuéry, P.; Harrowfield, J. Uranyl Ion Complexes with 1,1′-Biphenyl-2,2′,6,6′-Tetracarboxylic Acid: Structural and Spectroscopic Studies of One- to Three-Dimensional Assemblies. *Inorg. Chem.* **2015**, *54* (13), 6296–6305. https://doi.org/10.1021/acs.inorgchem.5b00596.

(21) Adelani, P. O.; Albrecht-Schmitt, T. E. Heterobimetallic Copper(II) Uranyl Carboxyphenylphosphonates. *Cryst. Growth Des.* **2011**, *11* (10), 4676–4683. https://doi.org/10.1021/cg200978y.

(22) Thuéry, P.; Harrowfield, J. Chiral One- to Three-Dimensional Uranyl-Organic Assemblies from (1R,3S)-(+)-Camphoric Acid. *CrystEngComm* **2014**, *16* (14), 2996–3004. https://doi.org/10.1039/c3ce42613k.

(23) Bai, R.; Chen, L.; Zhang, Y.; Chen, L.; Diwu, J.; Wang, X. F. The Presence of Mixed-Valent Silver in the Uranyl Phenylenediphosphonate Framework. *New J. Chem.* **2020**, *44* (15), 6037–6041. https://doi.org/10.1039/d0nj00573h.

(24) Thuéry, P.; Harrowfield, J. AgI and PbII as Additional Assembling Cations in Uranyl Coordination Polymers and Frameworks. *Cryst. Growth Des.* **2017**, *17* (4), 2116–2130. https://doi.org/10.1021/acs.cgd.7b00081.

(25) Thuéry, P.; Harrowfield, J. Modulation of the Structure and Properties of Uranyl Ion Coordination Polymers Derived from 1,3,5-Benzenetriacetate by Incorporation of Ag(I) or Pb(II). *Inorg. Chem.* **2016**, *55* (13), 6799–6816. https://doi.org/10.1021/acs.inorgchem.6b01168.

(26) Kerr, A. T.; Cahill, C. L. Postsynthetic Rearrangement/Metalation as a Route to Bimetallic Uranyl Coordination Polymers: Syntheses, Structures, and Luminescence. *Cryst. Growth Des.* **2014**, *14* (4), 1914–1921. https://doi.org/10.1021/cg500050q.

(27) Groom, C. R.; Bruno, I. J.; Lightfoot, M. P.; Ward, S. C. The Cambridge Structural Database. *Acta Crystallogr. Sect. B Struct. Sci. Cryst. Eng. Mater.* **2016**, *72* (2), 171–179. https://doi.org/10.1107/S2052520616003954.

(28) Knope, K. E.; Kimura, H.; Yasaka, Y.; Nakahara, M.; Andrews, M. B.; Cahill, C. L. Investigation of in Situ Oxalate Formation from 2,3-Pyrazinedicarboxylate under Hydrothermal Conditions Using Nuclear Magnetic Resonance Spectroscopy. *Inorg.*

Chem. **2012**, *51* (6), 3883–3890. https://doi.org/10.1021/ic3000944.

(29) Bruker. APEXIII. Bruker AXS Inc.: Madison, Wisconsin, USA 2020.

(30) Bruker. BIS. Bruker AXS Inc.: Madison, Wisconsin, USA 2020.

(31) SAINT Version 8.34a. Bruker AXS Inc. Madison, WI, WI 2013.

(32) Sheldrick, G. M. SADABS. University of Göttingen: Göttingen, Germany 2005.

(33) Sheldrick, G. M. A Short History of SHELX. *Acta Crystallogr. Sect. A* **2008**, *64*, 112–122. https://doi.org/10.1107/s0108767307043930.

(34) Huebschle, C. B.; Sheldrick, G. M.; Dittrich, B. ShelXle: A Qt Graphical User Interface for SHELXL. *J. Appl. Crystallogr.* **2011**, *44* (6), 1281–1284. https://doi.org/10.1107/s0021889811043202.

(35) Walker, N.; Stuart, D. An Empirical Method for Correcting Diffractometer Data for Absorption Effects. *urn:issn:0108-7673* **1983**, *39* (1), 158–166. https://doi.org/10.1107/S0108767383000252.

(36) CrystalMaker, 8.2.2 Ed. Crystal Maker Software Limited: Bicester, England 2009.

(37) Putz, H. Match! Phase Identification from Powder Diffraction. Crystal Impact: Bonn, Germany.

(38) Jakob, A.; Rüffer, T.; Schmidt, H.; Djiele, P.; Körbitz, K.; Ecorchard, P.; Haase, T.; Kohse-Höinghaus, K.; Frühauf, S.; Wächtler, T.; Schulz, S.; Gessner, T.; Lang, H. Disilver(I) Coordination Complexes: Synthesis, Reaction Chemistry, and Their Potential Use in CVD and Spin-Coating Processes for Silver Deposition. *Eur. J. Inorg. Chem.* **2010**, *2010* (19), 2975–2986. https://doi.org/10.1002/ejic.201000159.

(39) Frisch, M. J.; Trucks, G. W.; Schlegel, H. B.; Scuseria, G. E.; Robb, M. A.; Cheeseman, J. R.; Scalmani, G.; Barone, V.; Petersson, G. A.; Nakatsuji, H.; Li, X.; Caricato, M.; Marenich, A. V.; Bloino, J.; Janesko, B. G.; Gomperts, R.; Mennucci, B.; Hratchian, H. P.; Ortiz, J. V.; Izmaylov, A. F.; Sonnenberg, J. L.; Williams-Young, D.; Ding, F.; Lipparini, F.; Egidi, F.; Goings, J.; Peng, B.; Petrone, A.; Henderson, T.; Ranasinghe, D.; Zakrzewski, V. G.; Gao, J.; Rega, N.; Zheng, G.; Liang, W.; Hada, M.; Ehara, M.; Toyota, K.; Fukuda, R.; Hasegawa, J.; Ishida, M.; Nakajima, T.; Honda, Y.; Kitao, O.; Nakai, H.; Vreven, T.; Throssell, K.; Montgomery, J. A., J.; Peralta, J. E.; Ogliaro, F.; Bearpark, M. J.; Heyd, J. J.; Brothers, E. N.; Kudin, K. N.; Staroverov, V. N.; Keith, T. A.; Kobayashi, R.; Normand, J.; Raghavachari, K.; Rendell, A. P.; Burant, J. C.; Iyengar, S. S.; Tomasi, J.; Cossi, M.; Millam, J. M.; Klene, M.; Adamo, C.; Cammi, R.; Ochterski, J. W.; Martin, R. L.; Morokuma, K.; Farkas, O.; Foresman, J. B.; Fox, D. J. Gaussian 16, Revision B.01, Gaussian, Inc., Wallingford CT. **2016**.

(40) Weigend, F. Accurate Coulomb-Fitting Basis Sets for H to Rn. *Phys. Chem. Chem. Phys.* **2006**, *8* (9), 1057–1065. https://doi.org/10.1039/b515623h.

(41) Becke, A. D. Density-Functional Thermochemistry. III. The Role of Exact Exchange. *J. Chem. Phys.* **1993**, *98* (7), 5648–5652. https://doi.org/10.1063/1.464913.

(42) Di Pietro, P.; Kerridge, A. U-Oyl Stretching Vibrations as a Quantitative Measure of the Equatorial Bond Covalency in Uranyl Complexes: A Quantum-Chemical Investigation. *Inorg. Chem.* **2016**, *55* (2), 573–583. https://doi.org/10.1021/acs.inorgchem.5b01219.

(43) Di Pietro, P.; Kerridge, A. Assessing Covalency in Equatorial U–N Bonds: Density Based Measures of Bonding in BTP and Isoamethyrin Complexes of Uranyl. *Phys. Chem. Chem. Phys.* **2016**, *18* (25), 16830–16839. https://doi.org/10.1039/C6CP01273F.

(44) Weigend, F.; Ahlrichs, R. Balanced Basis Sets of Split Valence, Triple Zeta Valence and Quadruple Zeta Valence Quality for H to Rn: Design and Assessment of Accuracy. *Phys. Chem. Chem. Phys.* **2005**, *7* (18), 3297–3305. https://doi.org/10.1039/b508541a.

(45) Cao, X.; Dolg, M.; Stoll, H. Valence Basis Sets for Relativistic Energy-Consistent Small-Core Actinide Pseudopotentials. *J. Chem. Phys.* **2003**, *118* (2), 487–496. https://doi.org/10.1063/1.1521431.

(46) Cao, X.; Dolg, M. Segmented Contraction Scheme for Small-Core Actinide Pseudopotential Basis Sets. *J. Mol. Struct. THEOCHEM* **2004**, *673* (1–3), 203–209. https://doi.org/10.1016/j.theochem.2003.12.015.

(47) Küchle, W.; Dolg, M.; Stoll, H.; Preuss, H. Energy-Adjusted Pseudopotentials for the Actinides. Parameter Sets and Test Calculations for Thorium and Thorium Monoxide. *J. Chem. Phys.* **1994**, *100* (10), 7535–7542. https://doi.org/10.1063/1.466847.

(48) Bader, R. F. W. *Atoms in Molecules: A Quantum Theory*; Oxford University Press: Oxford, UK, 1990.

(49) Keith, T. A. AIMAll, Version 19.10.12. TK Gristmall Software: Overland Park, Kansas, USA 2019.

(50) Bondi, A. Van Der Waals Volumes and Radii. *J. Phys. Chem.* **1964**, *68* (3), 441–451. https://doi.org/10.1021/j100785a001.

(51) Lu, G.; Haes, A. J.; Forbes, T. Z. Detection and Identification of Solids, Surfaces, and Solutions of Uranium Using Vibrational Spectroscopy. *Coordination Chemistry Reviews*. Elsevier B.V. November 1, 2018, pp 314–344. https://doi.org/10.1016/j.ccr.2018.07.010.

(52) Pietro, P. Di; Kerridge, A. Assessing Covalency in Equatorial U–N Bonds: Density Based Measures of Bonding in BTP and Isoamethyrin Complexes of Uranyl. *Phys. Chem. Chem. Phys.* **2016**, *18* (25), 16830–16839. https://doi.org/10.1039/c6cp01273f.

(53) Surbella, R. G.; Cahill, C. L. The Exploration of Supramolecular Interactions Stemming from the [UO 2(NCS)4(H2O)]2- Tecton and Substituted Pyridinium Cations. *CrystEngComm* **2014**, *16* (12), 2352–2364. https://doi.org/10.1039/c3ce42106f.

(54) Denning, R. G. Electronic Structure and Bonding in Actinyl Ions and Their Analogs. *J. Phys. Chem. A* **2007**, *111* (20), 4125–4143. https://doi.org/10.1021/jp071061n.

(55) 4-Fluorobenzoic acid - Raman - Spectrum - SpectraBase https://spectrabase.com/spectrum/BpTGfQ8BFfF (accessed Mar 16, 2022).